STUDY OF EBULLATED-BED FLUID DYNAMICS FOR H-COAL. QUARTERLY PROGRESS REPORT NO. 4, APRIL 1, 1981-JUNE 30, 1981

AMOCO RESEARCH CENTER, NAPERVILLE, IL.
RESEARCH AND DEVELOPMENT DEPT

JUL 1981

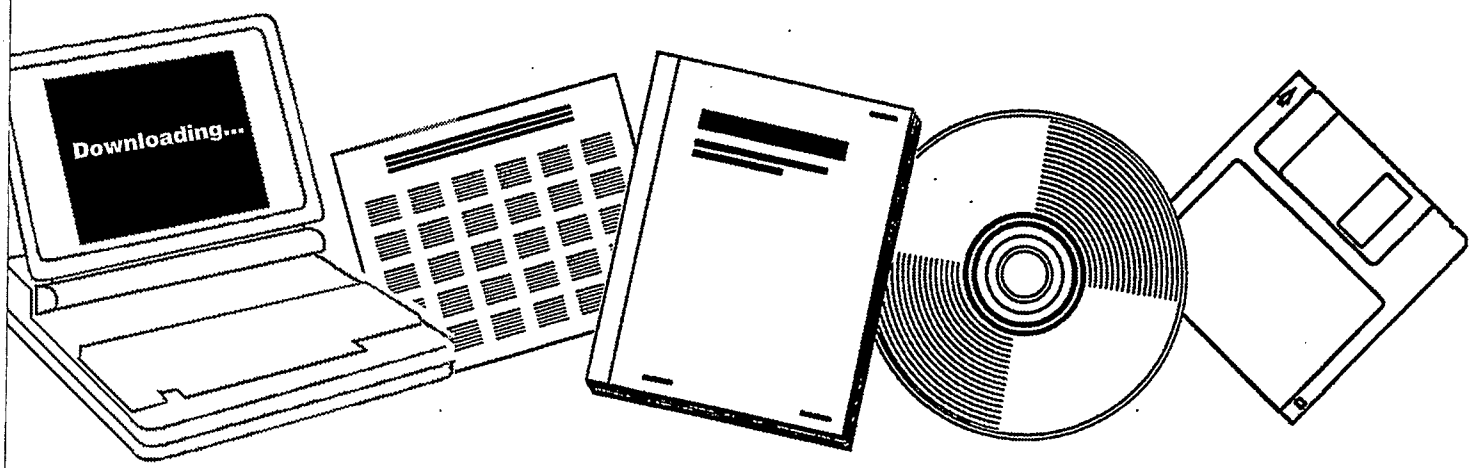

DOE/PC/30026-4

(DOE/PC/30026--4
DE82 008028)

80PC30026-4

STUDY OF EBULLATED-BED FLUID DYNAMICS FOR H-COAL

QUARTERLY PROGRESS REPORT NO. 4
APRIL 1, 1981-JUNE 30, 1981

R. J. SCHAEFER, D. N. RUNDELL

DATE PUBLISHED: JULY, 1981

CONTRACT DE-AC22-80PC30026

Research and Development Department
Amoco Oil Company
P. O. Box 400
Naperville, Illinois
60566

MASTER

STUDY OF EBULLATED BED FLUID DYNAMICS FOR H-COAL

QUARTERLY PROGRESS REPORT NO. 4
APRIL 1-JUNE 30, 1981

R. J. SCHAEFER, D. N. RUNDELL

AMOCO RESEARCH CENTER
NAPERVILLE, ILLINOIS 60566

PREPARED FOR THE UNITED STATES
DEPARTMENT OF ENERGY
UNDER CONTRACT DE-AC22-80PC30026

DATE PUBLISHED: JULY, 1981

TABLE OF CONTENTS

TABLE OF CONTENTS
-2-

FOREWORD

The H-Coal process, developed by Hydrocarbon Research, Incorporated (HRI), involves the direct hydroliquefaction of coal to low-sulfur boiler fuel or synthetic crude oil. The 200-600 ton-per-day H-Coal pilot plant is being operated next to the Ashland Oil, Incorporated, refinery at Catlettsburg, Kentucky, under DOE contract to Ashland Synthetic Fuels, Incorporated. The H-Coal ebullated bed reactor contains at least four discrete components: gas, liquid, catalyst, and unconverted coal and ash. Because of the complexity created by these four components, it is desirable to understand the fluid results of prior cold flow model experiments (1) to the operating H-Coal PDU reactor in Trenton, New Jersey. Studies are also planned to examine the coalescence behavior of gas bubbles in three-phase ebullated beds.

The work to be performed is divided into four parts: fluid dynamics measurements on the PDU reactor, gas bubble coalescence studies at Northwestern University, cold flow and mixing tests at Amoco's Naperville Research Center, and model implementation. The objective of this quarterly progress report is to outline progress in the first two areas.

SUMMARY

Battelle Institute completed characterization of fifteen slurry mix tank samples and issued the final technical progress report.

Cold flow measurements were initiated to study the fluid dynamics of coal char/kerosene slurries fluidizing a bed of HDS-2A catalyst. Tests were hampered by plugging of lines caused by coal fines agglomeration in several process lines. At higher gas flow rates, entrainment of gas down the recycle cup became significant. After seventeen tests were completed, the pilot plant testing was postponed in order to modify pilot plant piping.

Northwestern University continued development work on optical and electrical probes and began checkout of the laser holographic apparatus.

INTRODUCTION

The fluid dynamics of the H-Coal reactor has been previously studied in a cold flow unit. Reference 1 provides details of the construction of the unit and results of tests with a variety of gases, liquids, and catalyst sizes. A semi-theoretical model was developed to predict the volume fractions occupied by the gas, liquid, and catalyst phases. The aims of this new contract are fourfold:

1) The model developed using cold flow unit test results will be extended to apply to the operating H-Coal PDU reactor.

2) Because gas bubble dynamics are crucial in determining the nature of the flow, studies of bubble flow will be performed at Northwestern University using optically clear beds.

3) Liquid mixing tests will determine the residence time distribution of liquid in the reactor. Under the previous contract, it was determined that the coal char fines (simulating the unreacted coal and ash) were uniformly distributed throughout the bed. Hence, the measurement of liquid data is essential for modeling the residence time and kinetic parameters associated with the unreacted coal.

4) The model will be implemented into a readily usable format.

DATA COLLECTION

HRI PDU Fluid Dynamics Study

Viscosity of PDU Reactor Liquid.--The final report from Battelle Institute was received. With the exception of one sample bomb which was apparently empty on arrival, all samples were tested in the traveling bob viscometer. Some limited experiments were performed to measure the variation of

apparent viscosity with time at elevated temperatures. Battelle's final report is presented in Appendix A.

Amoco Cold Flow Fluid Dynamics Tests.--Cold flow three-phase fluidization tests were performed with a 4.3 vol% slurry of coal char in kerosene at ambient conditions. Gas, catalyst, and liquid slurry volume fractions were measured at various operating conditions. Six slurry samples were taken from various taps to verify the complete mixing of the coal char fines throughout the unit.

During these tests, it was necessary to keep liquid flowing through the recycle cup downcomer line (see Figure 1) to the slurry recycle pump to prevent coalescence and blockage by the coal fines. Mixing of this feed and a parallel feed from Separator D-3 through the slurry feed pump into the unit was hampered by interaction between the two pumps. The recycle pump, a positive-displacement pump, was overcoming the head of the centrifugal feed pump. Some experiments were performed by draining the separator and recycling all the slurry feed through the recycle cup. Gas entrainment in this recycle line hampered data collection at higher gas velocities, however.

The experimental program was suspended to permit repiping of the unit to the configuration shown in Figure 2.

Northwestern University/Gas Bubble Dynamics

Efforts continued at Northwestern University to develop both the light beam probes and impedance probes to measure bubble properties in small regions of the bed. Both probes and their associated electrical components have been fabricated. An initial analysis program to calculate bubble size and rise velocity distributions from experimental data was written. A trial holographc image was taken of the 6" glass column at a low gas rate; it was possible to measure the bubble sizes over the entire 6" cross-section.

Northwestern's three monthly progress reports appear in Appendix B.

Liquid Mixing Tests

The literature search for articles describing dispersion of liquid in three-phase fluidized beds was started. Possible experimental methods identified to date include organic dye tracers, UV fluorescence, radioactive tracers, or powdered iron tracers with piezoelectric detectors.

A 2" diameter plexiglass scale model of the cold flow unit was designed, and material was ordered for fabrication. The bench-scale unit will be employed to perform scoping experiments and verify techniques before final tests in the 6" diameter unit.

DATA ANALYSIS

HRI PDU Fluid Dynamics Study

Viscosity of PDU Reactor Liquid.--In June, Battelle repeated viscosity and density measuremetns on one sample (Amoco-15) to observe possible changes of these properties with time at elevated temperatures. In previous experiments, Battelle found the viscosity could be modeled by the expression for a Bingham plastic:

$$\underline{T} = \underline{T}_o + \eta_{pl} \dot{\gamma}$$

Figures 3-5 show that the viscosity and density were indeed changing with time at 700°K in the viscometer; all the previously reported temperature data therefore have an implicit parameter of time. Further analysis will be necessary to back-calculate the effective viscosity of these slurries in the H-Coal reactor.

Amoco Cold Flow Fluid Dynamics Tests.--The coal char concentrations of the six slurry samples taken from the unit are shown in Table I. With one exception (Sample 77-139-6), the values are similar within the expected range of variability.

Table II shows the measurements of gamma-ray attenuation in the line from the recycle cup. For Tests 11, 15, 16, and 17, the higher count rate indicates that gas was being entrained along with the liquid. Because gas velocity in the cold flow unit is calculated from the gas leaving the system, these tests should not be used for analysis.

Table III presents the catalyst bed expansion data. In Figure 6, these data are contrasted with earlier results from Run 204, where 5.1 vol% coal char fines was slurried in kerosene. Bed expansions for the current tests were consistently higher than for the earlier series. Possible reasons for this variation are under investigation. Tables IV and V summarize the holdups of gas and liquid in the dense (gas/liquid/catalyst) region and in the dilute phase above the catalyst bed.

PLANS FOR NEXT PERIOD

1) Continue studies at Northwestern University.

2) Continue literature search regarding liquid mixing.

3) Continue analysis of fluid dynamics data taken during PDU-10.

4) Continue cold flow experiments at Naperville using HDS-2A catalyst and kerosene/coal char slurries.

5) Begin scoping experiments with tracers to study liquid dispersion.

REFERENCES

1) I. A. Vasalos, et al., Final Progress Report, "Study of Ebullated Bed Fluid Dynamics for H-Coal," Contract DE-AC05-77ET-10149, February, 1980.

NOMENCLATURE

$\dot{\gamma}$	Shear rate	Sec^{-1}
η_{pl}	Plastic viscosity	$N \cdot S/m^2$
T	Shear stress in viscometer	N/m^2
T_o	Yield stress	N/m^2
ϵ	Volume fraction of component	
u	Superficial velocity	Ft/Sec
V_{CD}	Darton-Harrison drift flux	mm/Sec

Subscripts

b	Bed (dense) phase value
c	Catalyst
g	Gas
l	Liquid
γ	Determined by γ-ray absorption
ΔP	Determined by ΔP measurement.

TABLE I

COAL CHAR CONCENTRATIONS, RUN 221

Sample ID	Sample Location	Coal Char Concentration, Wt%
AU-77-135-2	Base of line from recycle cup	6.42
AU-77-136-3	First spool piece (reactor base)	6.52
AU-77-137-4	Second spool piece (60" from reactor base)	6.38
AU-77-138-5	Third spool piece (120" from reactor base)	6.40
AU-77-139-6	Fourth spool piece (180" from reactor base)	6.78
AU-77-140-7	Reactor overhead line	6.35

DNR/ml
7/15/81

TABLE II

GAMMA-RAY MEASUREMENT OF GAS IN RECYCLE LINE

Test	U_g, Ft/Sec	U_l, Ft/Sec	γ-Ray Intensity Recycle Line, c/Sec
221-1	0.078	0	199
2	0.077	0	199
3	0.104	0	203
4	0.144	0	199
5	0.154	0	207
6	0.169	0	201
7	0.169	0	199
8	0.056	0.094	206
9	0.056	0.099	207
10	0.056	0.075	200
11	0.048	0.120	217*
12	0.078	0.048	202
13	0.079	0.075	207
14	0.104	0.047	205
15	0.125	0.048	209*
16	0.148	0.049	225*
17	0.081	0.076	210*

*Excess gas.

DNR/ml
7/15/81

TABLE III

% BED EXPANSION FOR RUN 221

Catalyst: HDS-2A
Gas: Nitrogen
Liquid: Kerosene
Coal Char Concentration: 4.3 Vol%
Temperature: 73°F

Run No.	Liquid Flow Rate, Ft/Sec	Gas Flow Rate FT/Sec	Catalyst Bed Height (Inches)	% Bed Expansion
221-1	0.05	0.0	54	17
2	0.08	0.0	56	22
3	0.10	0.0	65	41
4	0.13	0.0	72	57
5	0.15	0.0	78	70
6	0.18	0.0	89	93
7	0.21	0.0	103	124
8	0.05	0.05	52	13
9	0.05	0.10	52	13
10	0.05	0.07	52	13
12	0.08	0.05	58	27
13	0.08	0.07	67	45
14	0.10	0.05	66	43

DNR/ml
7/15/81

TABLE IV

CALCULATED HOLDUPS, RUN 221: DENSE PHASE

CATALYST : HDS2A
GAS : NITROGEN
LIQUID : KEROSENE
COAL CHAR CONC: 4.3 VOL %
TEMPERATURE : 73. DEG F

Run No.	Liquid Flow Rate, Ft/Sec	Gas Flow Rate, Ft/Sec	ϵ_{CB}	ϵ_{l},%B	ϵ_{l},APB	ϵ_{g},%B	Vcd (Mm/Sec
221- 1	0.052	0.0	0.47	0.51	1.72	0.0	0.0
- 2	0.077	0.0	0.45	0.52	1.78	0.0	0.0
- 3	0.104	0.0	0.39	0.58	0.38	0.0	0.0
- 4	0.129	0.0	0.35	0.62	1.73	0.0	0.0
- 5	0.154	0.0	0.32	0.64	0.64	0.0	0.0
- 6	0.181	0.0	0.28	0.68	0.67	0.0	0.0
- 7	0.208	0.0	0.25	0.72	0.70	0.0	0.0
- 8	0.052	0.050	0.49	0.37	0.26	0.12	9.1
- 9	0.051	0.099	0.49	0.35	0.24	0.15	20.3
-10	0.051	0.075	0.49	0.36	0.21	0.14	14.5
-12	0.077	0.048	0.43	0.43	0.37	0.11	7.9
-13	0.077	0.075	0.38	0.48	0.44	0.12	15.2
-14	0.104	0.047	0.38	0.49	0.45	0.10	7.3

TABLE V

CALCULATED HOLDUPS, RUN 221--DILUTE PHASE

CATALYST : HDS2A
GAS : NITROGEN
LIQUID : KEROSENE
COAL CHAR CONC: 4.3 VOL %
TEMPERATURE : 73. DEG F

Run No.	Liquid Flow Rate, Ft/Sec	Gas Flow Rate, Ft/Sec	ε_l, γ	$\varepsilon_l, \Delta P$	ε_g, γ
221- 1	0.052	0.0	0.96	0.92	0.0
- 2	0.077	0.0	0.95	0.92	0.0
- 3	0.104	0.0	0.96	1.65	0.0
- 4	0.129	0.0	0.97	1.67	0.0
- 5	0.154	0.0	0.95	0.92	0.0
- 6	0.181	0.0	0.96	0.92	0.0
- 7	0.209	0.0	0.95	0.92	0.0
- 8	0.052	0.050	0.88	0.92	0.08
- 9	0.051	0.099	0.81	0.85	0.16
-10	0.051	0.075	0.84	0.88	0.12
-12	0.077	0.048	0.87	0.91	0.09
-13	0.077	0.075	0.80	0.85	0.16
-14	0.104	0.047	0.85	0.89	0.11

Figure 1

SCHEMATIC DIAGRAM OF COLD FLOW FLUID DYNAMICS UNIT

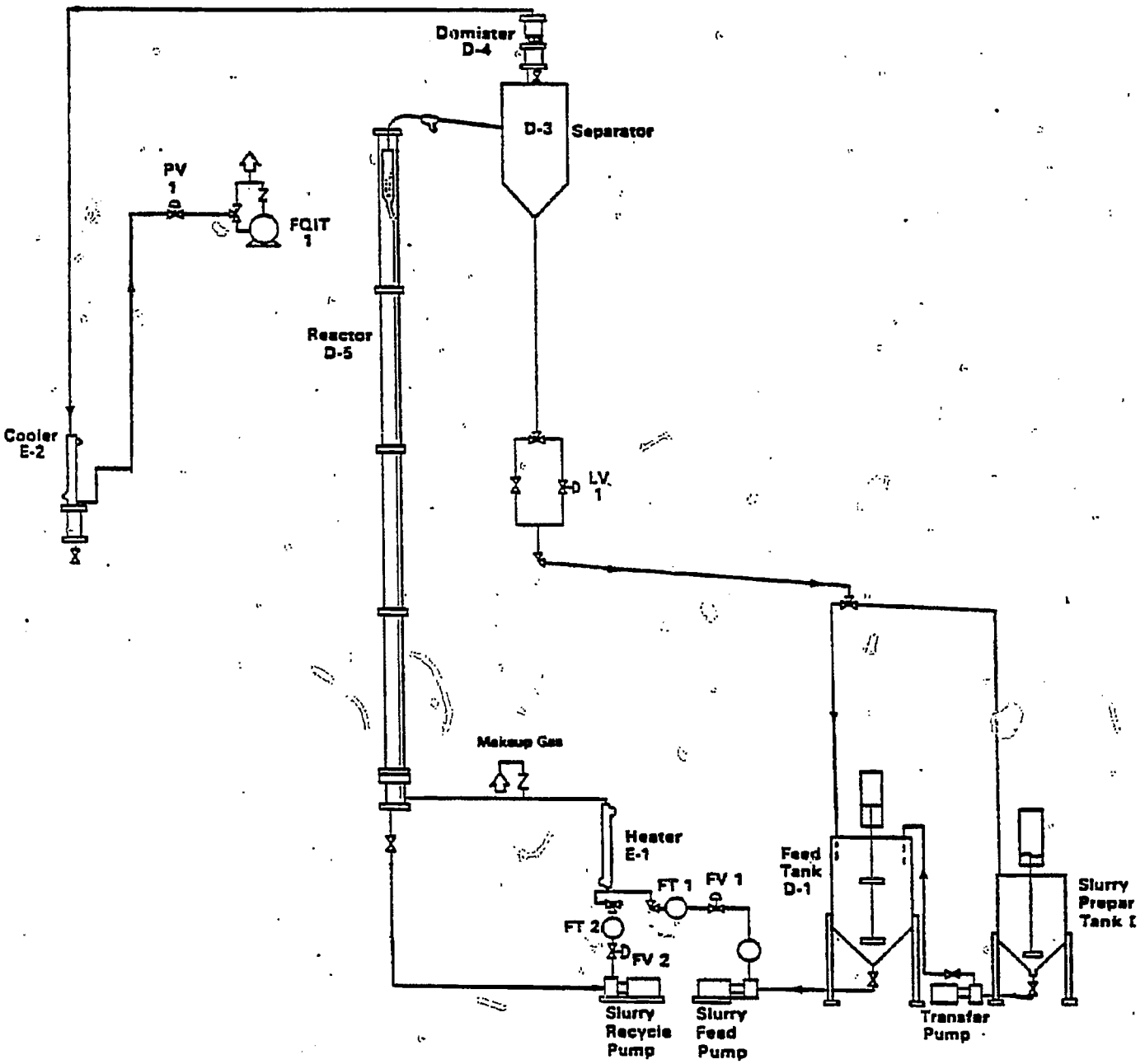

Figure 2

NEW PIPING CONNECTION DIAGRAM FOR COLD FLOW FLUID DYNAMICS UNIT

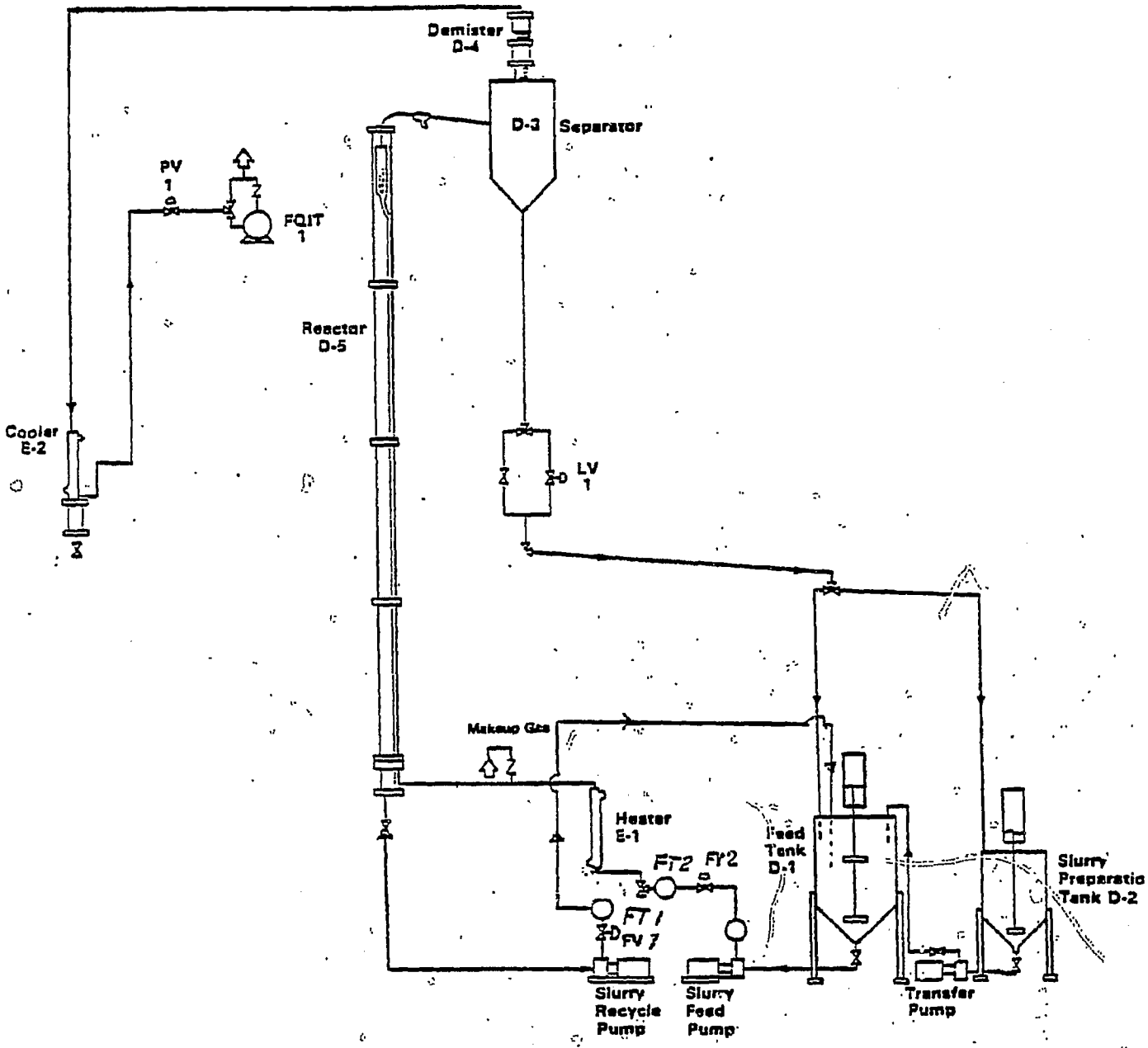

Figure 3

CHANGE OF DENSITY WITH TIME:
PDU LIQUID SAMPLE AMOCO-15

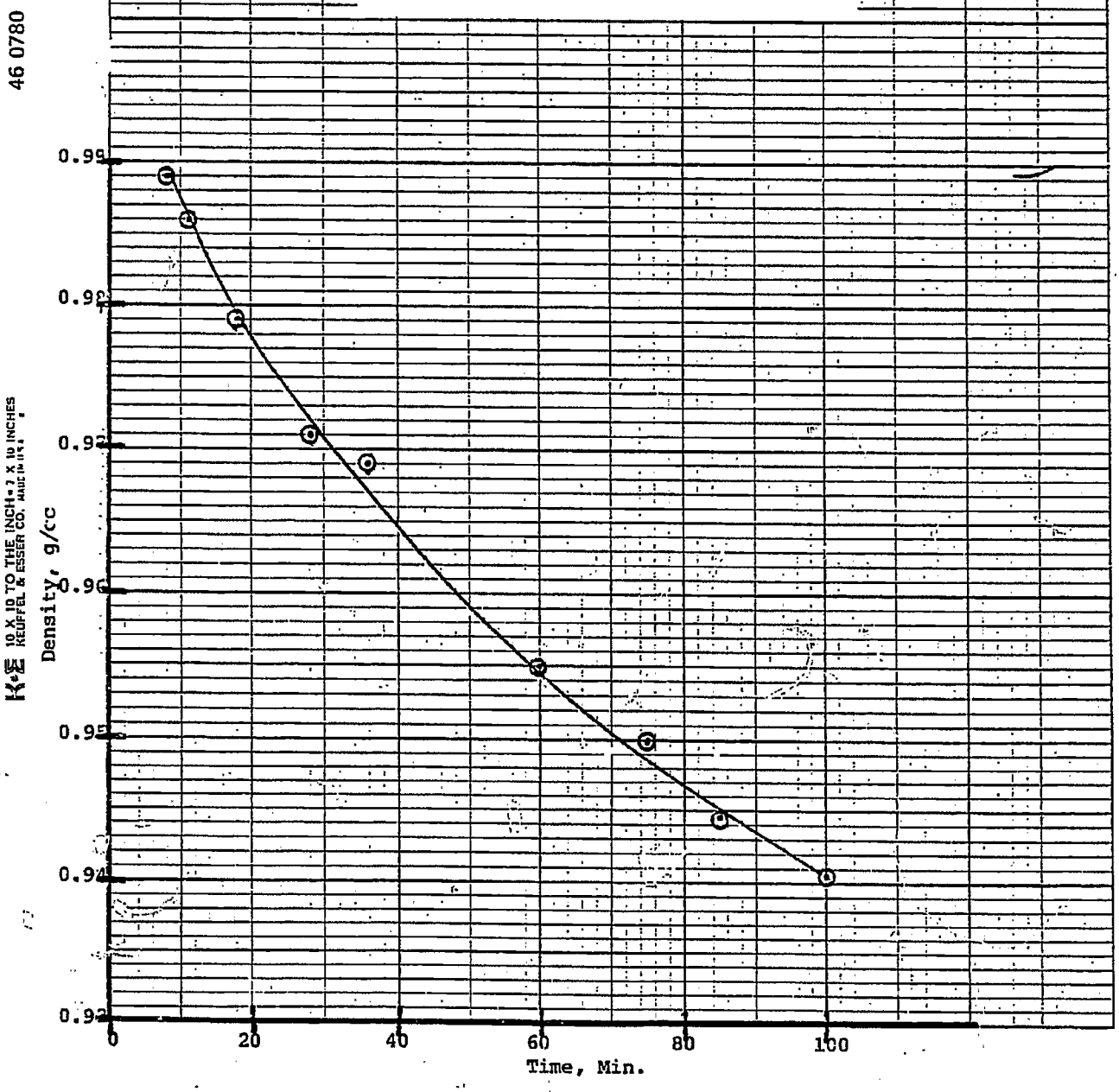

Figure 4

CHANGE OF PLASTIC VISCOSITY
WITH TIME:
PDU LIQUID SAMPLE AMOCO-15

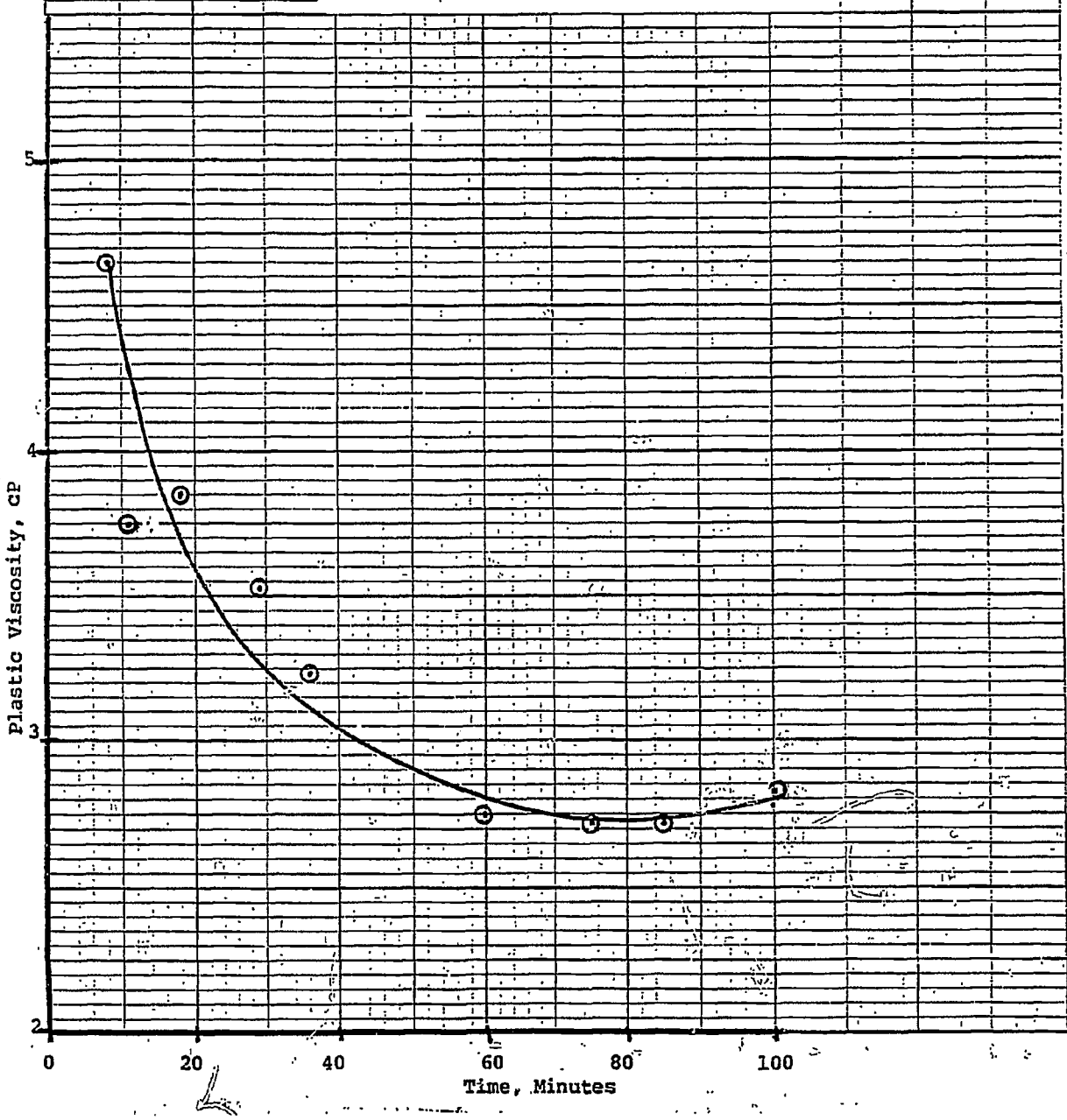

Figure 5

CHANGE OF YIELD STRESS
WITH TIME:
PDU LIQUID SAMPLE AMOCO-15

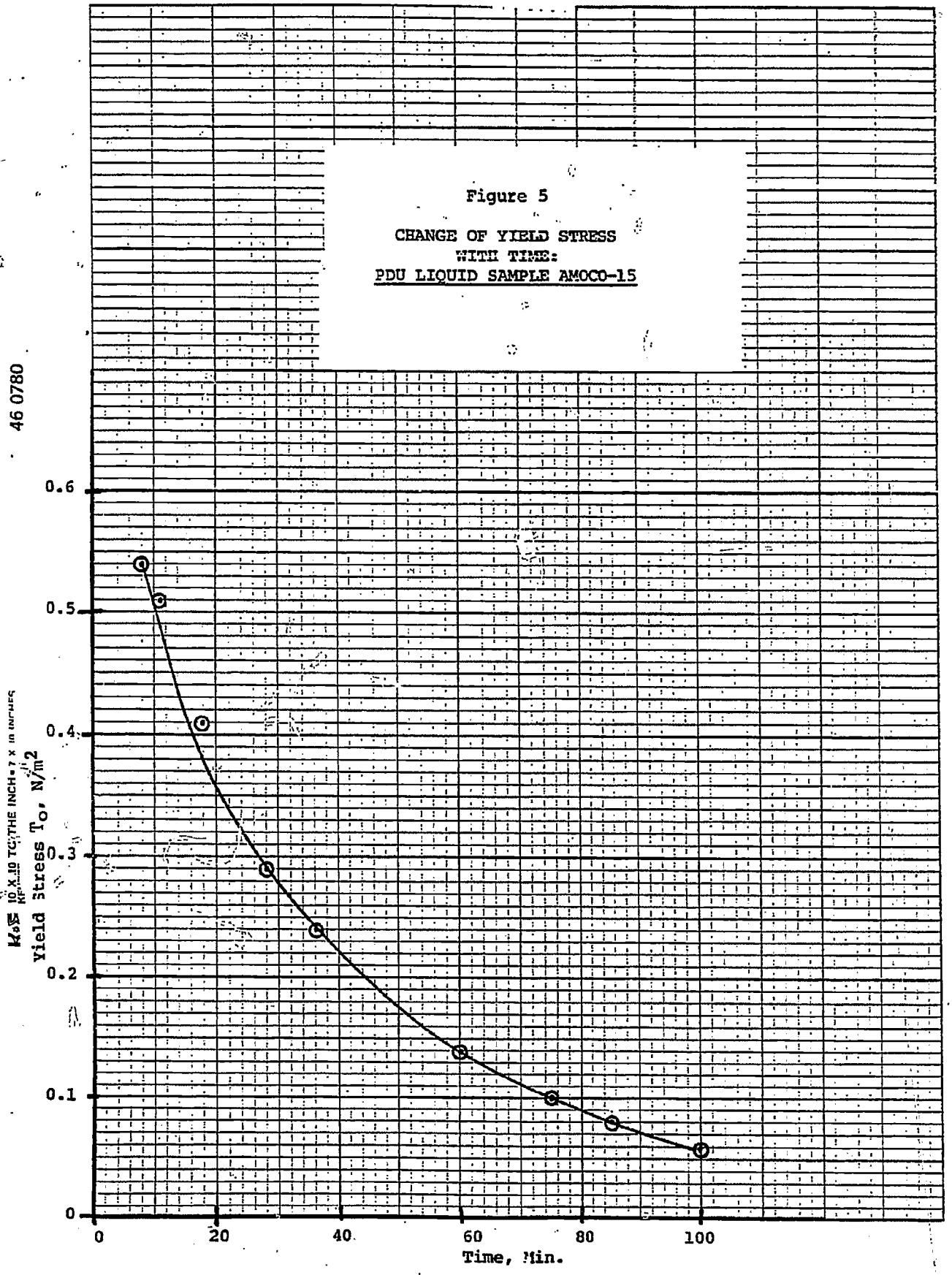

Figure 6

PER CENT BED EXPANSION:
RUN 221 VS. RUN 204

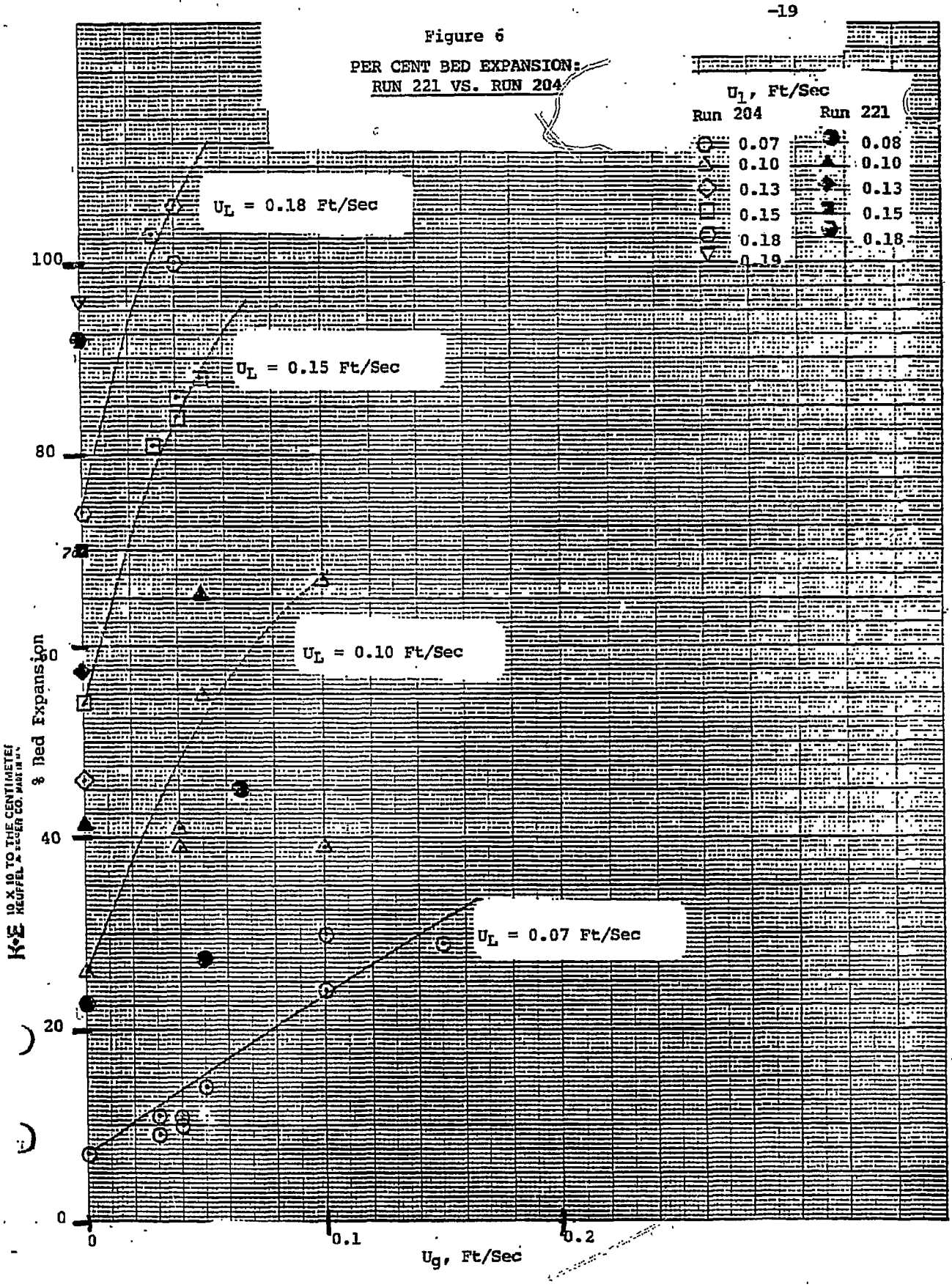

APPENDIX A

BATTELLE INSTITUTE FINAL REPORT

FINAL REPORT

on

VISCOSITY OF H-COAL SAMPLES

to

AMOCO OIL COMPANY

June 30, 1981

by

J. W. Droege, D. R. Taylor,
and S. P. Chauhan

BATTELLE
Columbus Laboratories
505 King Avenue
Columbus, Ohio 43201

TABLE OF CONTENTS

LIST OF TABLES

LIST OF FIGURES

VISCOSITY OF H-COAL SAMPLES

by

J. W. Droege, D. R. Taylor,
and S. P. Chauhan

June 30, 1981

ABSTRACT

The rheological properties of 14 samples taken from the H-COAL pilot plant have been determined at temperatures up to 725 K (845 F), mostly at a pressure of 17.24 MPa (2500 psia) of hydrogen. The samples showed Bingham-plastic behavior. It was found that the properties were time-dependent in that the yield stress decreased to near zero. The rate of this change was higher at higher temperatures. Most measurements were made without regard to this time dependency. Therefore the results at the highest temperatures are somewhat in doubt for this reason.

INTRODUCTION

On December 11, 1979, Battelle submitted its report to AMOCO on measurements made on a few H-COAL samples. On April 25, 1980, we submitted our proposal for more measurements and the current program got under way on September 18, 1980.

The objective of this research was to determine the rheological properties of 15 samples to be supplied by AMOCO. The samples were to be collected without exposure to air and were to be transferred into our apparatus without exposure to air. Measurements were to be made of a suitabl range of shear rates at temperatures between 350 and 450 °C under hydrogen pressures of 2000 to 3000 psi.

It was not expected that the properties would change appreciably with time, but the possibility was recognized. Therefore measurements were begun at lower temperatures and continued at higher temperatures until the series was complete. With some of the samples repeat measurements were made

at lower temperatures after completing the high-temperature work. Some of the samples were maintained for a while at one temperature to check on the constancy of results. It became apparent that the results were indeed time-dependent. Since extensive constant-temperature measurements with extrapolation to zero time would have required large samples and a lot of time, only one such measurement was made in this manner, by way of illustration.

RHEOLOGY

Most of the work on rheology of coal-derived liquids has been done at atmospheric pressure and therefore not far above room temperature. Viscosities of concentrated slurries were found to be non-Newtonian and to be generally higher than predicted for spherical particles.[1] Coal-oil suspensions made with brown coal have been found to increase in viscosity with aging, even at room temperature.[2] The viscosity of coal-derived liquids has been related to asphaltene and preasphaltene content.[3,4] Aging of coal-derived liquids, especially in the presence of oxidizing gases, has been found to increase viscosity.[5]

A few attempts have been made to measure viscosity at elevated temperature and pressure. In a continuing program at Oak Ridge National Laboratory a continuous coal-liquids flow system has been instrumented for measurement of viscosity and density.[6] The slurry is pumped through a length of heated tubing after which it passes through a constant-temperature section equipped with pressure taps. By varying the flow rate it is possible to vary shear stress and shear rate and thus to study the rheology of non-Newtonian mixtures. Since the residence time in the heated tubing is short, the viscosity of newly made sample can be determined.

Viscometer

A reciprocating concentric-cylinder viscometer was developed at Battelle for measuring the viscous properties of Synthoil liquids at elevated temperature and pressure.[7] It seemed well suited for the present

measurements. The mechanical system is simple. There is little loss due to friction. The reciprocating action of the inner cylinder, the "bob", tends to keep the sample mixed. Data can be obtained quickly. The bob can be operated over a wide range of shear rates.

The apparatus is shown in Figure 1. It depends on the axial movement of concentric cylinders resulting in a pumping action which forces liquid to flow in the direction opposite to that of the inner cylinder in the space between the cylinders. A mixing autoclave, shown on the right, can be used to hold the sample at a controlled temperature prior to transfer into the viscometer.

A 0.3L autoclave constitutes the outer cylinder of the viscometer. A cylindrical bob (9) has a radius approximately 1-mm less than the inside radius of the autoclave. The bob is attached by tubing through a connector (6) to a large Alnico V bar magnet (5) and, by means of a thin rod, to a second smaller bar magnet (3). The magnets move freely inside tubing extending from the top of the autoclave. The bob is hollow, the space inside communicating with the autoclave atmosphere through the suspension tube. Outside the pressure system are located two large coils (4). When a current is passed through these two coils in opposite directions, an upward or downward force is exerted on the bob, depending on the direction of current flow. A second pair of coils (2) surrounds the smaller magnet. Motion of this magnet induces a current in these coils whereby the direction and rate of motion of the bob are detected. A vibrator helps to keep the bob moving smoothly.

Good temperature control is important. Because of the high heat capacity of the system it is important that the heaters be closely coupled to the metal of the autoclave. A sheathed heater is brazed to the body of the viscometer. It provides the primary temperature control. A control thermocouple is inserted into the bottom of the autoclave where it makes good contact with the metal. A three-action proportional controller is used. Two band heaters are used, one around the flange, the other around the cover, independently controlled to keep these parts at the same temperature as the body of the autoclave. A copper enclosure around the valves below the autoclave (10) is provided with strip heaters to keep the valves

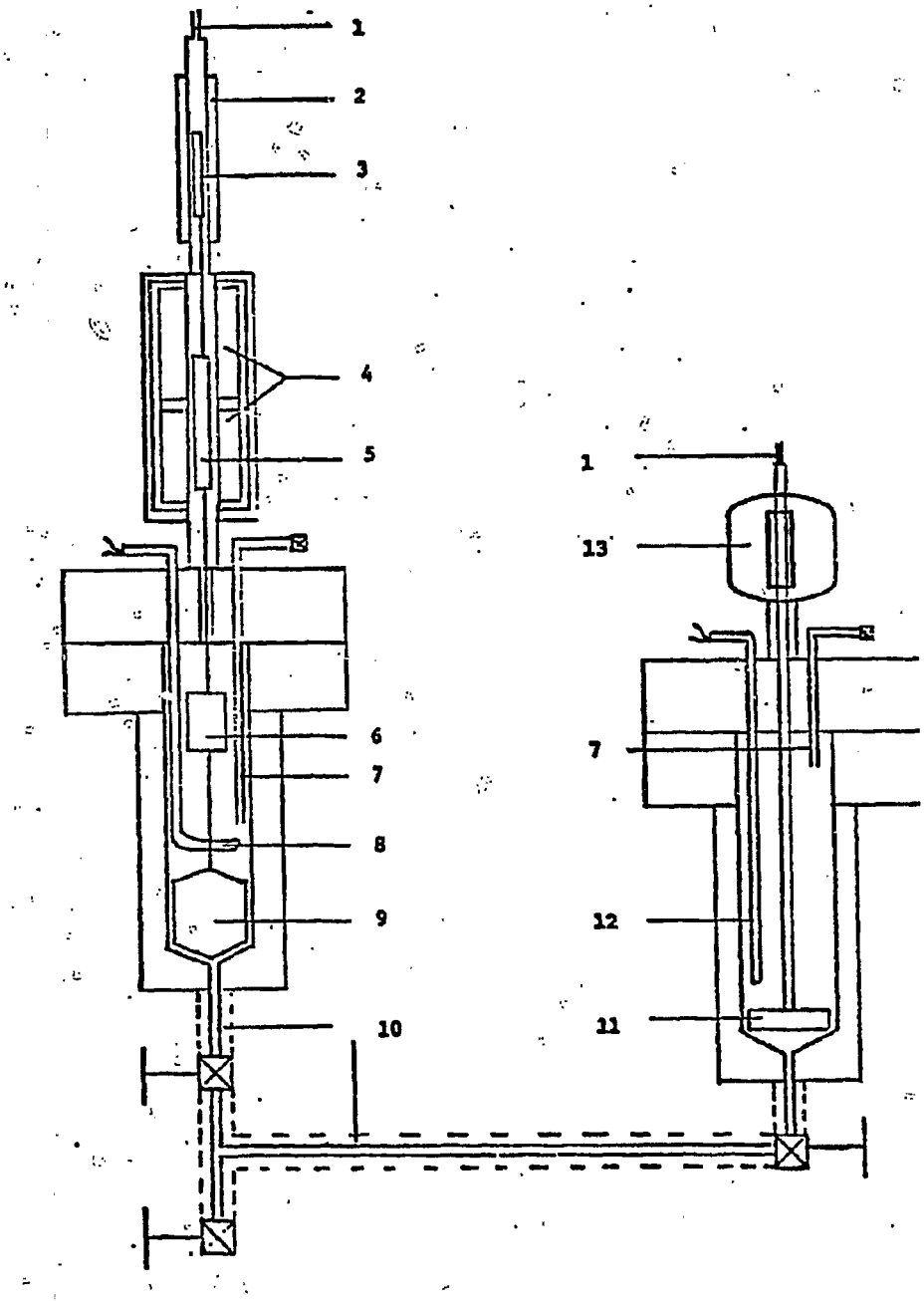

FIGURE 1. VISCOMETER AND MIXING AUTOCLAVE

and tubing at the same temperature. The principal heat leak is through the water-cooled tube extending out the top of the autoclave. Its cooling effect is well compensated by the band heaters. A sheathed thermocouple (8), immersed in the sample just above the bob, shows the sample temperature. A similar temperature-control system keeps the preheater autoclave at constant temperature.

Valves and 1/4-in. tubing are provided, as shown, by which sample can be transferred from one autoclave to the other. Ports for the introduction and withdrawal of gas, for pressure measurement and control and for a safety valve are provided, several of which are shown (1,7). A sensitive back-pressure regulator controls the pressure. The mixing autoclave is stirred with a magnetically driven (13) turbine-type agitator (11). The viscometer autoclave is stirred only by the action of the bob. As an aid in keeping the solids in suspension, a burst of gas is occasionally admitted from below.

Procedure

The viscosity of a fluid in the apparatus can be calculated from the velocity and force acting on the bob. The equations have been worked out for Newtonian liquids.[7,8] The force applied to the bob was derived by calibration from the current passed through the lifting coils. From this calibration and from the dimensions of the apparatus the current scale could be converted to a shear-stress scale. The zero on this shear-stress scale was not easily established, since some force was required to keep the bob just suspended in the liquid. This force was related to the mass of the bob assembly and to the density of the liquid. For liquids not departing greatly from Newtonian behavior, the zero on the shear-stress scale could be estimated from data obtained with both a rising and a falling bob. From this value and from a knowledge of the volume of the bob, the density could be calculated. Shear rate was related to bob velocity through a calibration with a Newtonian standard.

Figure 2 shows a sample plot of shear stress versus shear rate. A force equivalent to about 3.65 on the shear-stress axis was required to overcome gravity in this instance. Two sets of points are shown, one for

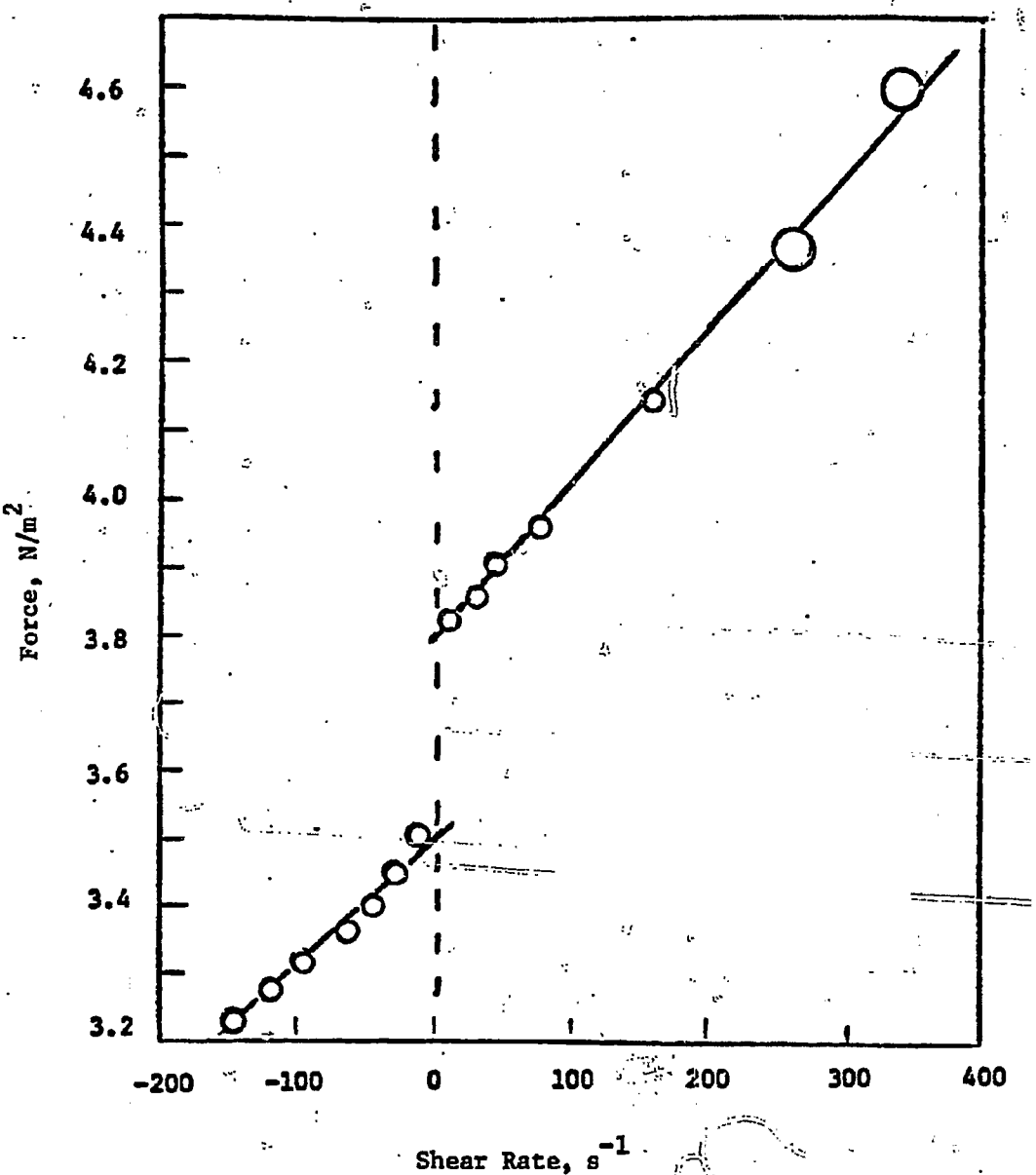

FIGURE 2. SAMPLE DATA

a rising, the other for a falling bob. The gap between the two intercepts at zero shear rate is a measure of the yield stress. It will be seen that the data follow the Bingham-plastic model. The viscous behavior is characterized by two constants, as follows:

$$\tau = \tau_o + \eta_{pl} \dot{\gamma}, \qquad (1)$$

where τ_o is the dynamic stress and η_{pl} is the "plastic viscosity", that is, that is, the slope of the line of Figure 2. The self-centering behavior of the bob works better on the rising stroke, therefore, results were based mostly on the upper line. Most of the data were obtained at shear rates between 10 and 100 s^{-1}.

When good data were obtained both with a rising and a falling bob, the point on the stress axis corresponding to a balanced bob could be determined (3.65 in Figure 2). This corresponds to a determination of the weight of the bob immersed in the liquid. A similar determination for the bob suspended in air and a determination of the volume of the bob are all that are needed for a density determination. This procedure was used for the density determinations shown. The procedure was not very successful at 400 K but appeared to give reliable results at higher temperatures.

The procedure for loading samples into the viscometer was as follows. The AMOCO sample bulb, wrapped with heating tape and insulation, was mounted vertically beside the apparatus shown in Figure 1. The valves at the bottom were connected with 1/4-in. tubing. The valve at the top of the sample bulb was connected to a low-pressure hydrogen supply and to a vent through a bubbler. Both autoclaves were first evacuated and flushed with hydrogen. After warming the sample to about 350 K the pressure in the sample bulb was relieved. Then a stream of hydrogen was passed up through the sample to provide some mixing.

The transfer was begun by applying a small pressure (about 20 psig) to the top of the sample bulb as well as to the mixing autoclave, opening connecting valves, then bleeding gas slowly from overflow tube 7 in the mixing autoclave. When the liquid level reached the overflow tube the flow of gas stopped and the connecting valve below this autoclave was closed. Hydrogen was then passed from the viscometer autoclave into the mixing autoclave to clear the connecting tube. The mixing autoclave now contained about 300 cm^3 of sample, a little more than three times as much

as the required sample. The charge was stirred vigorously for a time to homogenize the sample. Sample was then transferred in a similar way into the viscometer until it rose to the level of overflow tube 7 in this autoclave. Excess sample was blown out this overflow tube, thus leaving a sample of the required volume in the viscometer. Unused sample from the mixing autoclave was then transferred back into the sample bulb where it was kept with an overpressure of about 50 psig of hydrogen.

Before beginning the measurements the pressure in the viscometer was increased to the desired level, then the temperature of the viscometer was raised to the temperature chosen for the first measurements. After making the necessary measurements, the viscometer and contents were raised to the next higher temperature until the work was completed. At the conclusion of the measurement the sample was drained from the autoclave and discarded.

On several occasions we departed from the standard procedure, either intentionally or out of necessity. The exceptions will be described by sample number:

- AMOCO 1, 2, and 3. For these samples the pressure was increased and decreased throughout the run in an attempt to find the effect of pressure. These pressure changes were not made at the highest temperatures for fear of losing volatiles with the venting gas.
- AMOCO 3. Because of the formation of a plug in the transfer line, it was not possible to return sample to the sample bulb. The sample used for the measurements was subsequently removed through the top of the viscometer and, after exposure to air, was returned to the sample bulb.
- AMOCO 7. This was the sample chosen for our first measurements. We developed a plug during the first attempt to transfer. The sample was contaminated with air and water and some of it was evaporated after overheating. After the measurements we had trouble draining the sample and damaged our bob, which had not been properly calibrated. Therefore this run was declared to be a total loss.
- AMOCO 8. At the end of the second run with this sample we judged that no unused sample remained in the mixing autoclave. We therefore transferred the sample used for the measurements back into the sample bulb.

- AMOCO 12. There appeared to be insufficient sample for a full charge to the viscometer although apparently normal data were obtained. The sample was returned to the sample bulb after the measurements.
- AMOCO 13. We could find no sample in this bulb. Therefore, we presume the sample bulb now to be empty.
- AMOCO 15. In order to make one good observation of the effect of time on our results, a second measurement was made with this sample using a modified procedure. The overflow tube 7 in the mixing autoclave was lengthened so that a sample of the required size could be introduced into this autoclave. After making this transfer the autoclaves were both pressurized to 17.24 MPa (2500 psi) and the viscometer (but not the mixing autoclave) was heated to 700 K. The cold sample was then transferred to the preheated autoclave where it was heated rapidly to the measurement temperature. Data were recorded at 700 K for an hour and a half. Subsequently measurements were made at lower temperatures.
- AMOCO 16. We apparently encountered a plug in the line and found transfer difficult. We were unable to return sample to the sample bulb and presume that the sample bulb is now empty.

The viscometer, which had been performing acceptably at higher viscosities, gave data with a lot of scatter with these specimens. Presumably this was due to frictional effects, which represent a much more serious problem at low viscosities than at higher. During January, 1981, we made some vigorous attempts to correct these frictional problems.

For our bob to move up and down within the autoclave without friction requires good alignment. We had been relying on a flexible joint which allowed the bob to center itself in the autoclave even if the magnet assembly was not perfectly aligned. During January we made the following changes:

(1) A tool was devised which enabled us to align the axis of the magnet housing accurately with the axis of the autoclave

(2) One of the guides which kept the magnet assembly running true was removed. This eliminated one possible source of friction.

(3) The flexible joint was replaced with a fixed connector.

(4) The system was calibrated over the range of 0.3 to 33 mPA•s (cP).

The calibrations, which were based on the known viscosities of five liquids, were in satisfactory agreement. The scatter in the measurements on coal liquids was greatly reduced.

We believe that the older data, while flawed by excessive scatter, were otherwise valid. However the quality of data improved, beginning with AMOCO 4, run in late January, and subsequent determinations will be considered more reliable. Most of the measurements made prior to that time were subsequently repeated.

Results

The results of our measurements are shown in Table 1. Within each set of measurements on a single sample the results are shown in the order in which they were obtained. In most cases the first measurement was made at about 400 K. This routine was established in order to show gross differences from sample to sample, since measurements are more easily made at higher viscosities. The results show that there was the expected relationship between viscosities at lower and at higher temperatures, but there were also many departures from this relationship.

The accuracy of these results is plainly not high. It is difficult to place a numerical estimate on the uncertainty. Perhaps the best assessment would come from the numerous repeat determinations and comparisons with work at ORNL. These comparisons will be discussed in a subsequent section.

In almost all cases the data followed the relationship corresponding to Bingham plastic behavior. At low shear rates, of the order of 10 s^{-1}, shear rates often appeared to be higher than the Bingham-plastic straight line would predict. This may be an artifact of the measurement or it may indicate that the true behavior is somewhere between pseudoplastic and Bingham plastic.

TABLE 1. VISCOUS PROPERTIES OF AMOCO SAMPLES

Temperature, K	Temperature, °F	Pressure, MPa	Pressure, psia	Elapsed Time, min	Viscosity η_{pl}, mPa·s	Yield Stress, τ_o N/m²	Density, kg/m³
				AMOCO 1 (March)			
408.2	275.0	17.24	2500		10.4	.20	1065
625.5	666.1	13.79	2000		2.07	.05	909
624.9	665.1	17.24	2500		2.15	.04	907
625.2	665.6	20.69	3000		2.03	.03	901
648.5	707.5	13.79	2000		1.87	.06	881
649.2	708.8	17.24	2500		1.87	.05	884
648.9	708.3	20.69	3000		1.84	.04	882
673.2	752.0	20.69	3000		1.77	.08	858
673.5	752.5	17.24	2500		1.77	.08	858
673.2	752.0	13.79	2000		1.71	.08	862
699.2	798.8	17.24	2500		1.73	.09	828
724.0	843.4	17.24	2500		1.33	.13	766
673.2	752.0	17.24	2500		1.84	.06	832
				AMOCO 1 (November)			
413.4	284.4	17.24	2500		8.8	.13	1033
623.5	662.5	13.79	2000		1.76	.06	900
624.3	664.0	17.24	2500		1.72	.02	899
624.8	664.9	20.69	3000		1.72	.01	897
645.3	701.8	13.79	2000		1.45	.12	869
645.7	702.5	17.24	2500		1.63	.13	870
646.2	703.4	20.69	3000		1.46	.11	870
669.2	744.8	13.79	2000		1.81	.12	856
698.2	797.0	17.24	2500		1.55	.08	818
723.2	842.0	17.24	2500	4	1.28	.16	762
722.7	841.1	17.24	2500	18	1.68	.24	755
723.1	841.8	17.24	2500	26	1.87	.32	750
723.2	842.0	17.24	2500	34	2.03	.33	755
				AMOCO 2 (May)			
406.6	272.3	17.24	2500		16.6	.26	1080
626.2	667.4	↓	↓		2.10	.10	913
648.2	707.0				1.92	.13	895
672.4	750.7				2.01	.15	844
672.2	750.2			37	1.92	.13	849
697.4	795.6			67	1.81	.20	804
725.0	845.2			97	1.76	.20	763
				AMOCO 2 (December)			
405.2	269.6	17.24	2500		14.0	.31	1107
627.0	668.8	13.79	2000		2.18	.07	925
627.2	669.2	17.24	2500		2.07	.05	932
626.6	668.3	20.69	3000		1.98	.09	926
646.0	703.2	13.79	2000		1.57	.11	903
646.6	704.3	17.24	2500		1.82	.13	899
648.2	707.0	20.69	3000		1.91	.09	900
672.6	751.1	17.24	2500		1.38	.17	865
696.2	793.4	17.24	2500		1.60	.18	836
719.6	835.7	17.24	2500		1.53	.23	798
				AMOCO 3 (March)			
409.0	276.4	17.24	2500		80.2	2.0	
627.0	668.8	13.79	2000		5.81	.42	995
627.3	669.4	17.24	2500		5.53	.42	996
627.2	669.2	20.69	3000		5.60	.42	1000
627.4	669.6	17.24	2500		5.23	.35	985
622.7	661.1	13.79	2000		5.22	.37	993
649.5	709.3	13.79	2000		5.00	.39	979
650.2	710.6	17.24	2500		4.97	.38	977

TABLE 1. (Continued)

Temperature K	Temperature °F	Pressure MPa	Pressure psia	Elapsed Time, min	Viscosity η_{pl} mPa·s	Yield Stress, τ_o N/m^2	Density, kg/m^3
				AMOCO 3 (March) (Continued)			
650.0	710.2	20.69	3000		4.94	.35	973
673.4	752.4	20.69	3000		3.58	.32	944
673.2	752.0	17.24	2500		3.52	.29	941
672.8	751.3	13.79	2000		3.70	.28	945
699.0	798.4	13.79	2000		2.95	.22	911
699.0	798.4	17.24	2500		2.65	.20	905
699.0	798.4	20.69	3000		2.77	.18	900
723.2	842.0	17.24	2500		2.20	.14	875
699.1	798.6	17.24	2500		2.11	.07	902
409.6	277.5	17.24	2500		46.3	.00	1093
				AMOCO 4 (May)			
407.6	274.1	17.24	2500	0	44.5	1.52	1069
622.2	660.2	↓	↓	80	3.46	.22	968
646.6	704.3			120	3.13	.22	952
646.2	703.4			190	3.11	.18	950
672.2	750.2			230	2.78	.15	925
698.2	797.0			250	1.85	.16	896
722.7	841.2			280	1.72	.08	863
722.8	841.5			288	1.60	.07	865
722.6	841.1			316	1.31	.00	859
722.6	840.9			345	1.32	.01	861
722.6	840.9			381	1.31	.01	860
				AMOCO 4 (January)			
407.2	273.2	13.79	2000		31.8		
626.2	667.6	↓	↓		3.65	.18	958
649.2	708.8				3.51	.18	942
673.6	752.7				2.78	.20	922
697.4	795.7				2.12	.20	896
722.4	840.7				1.74	.09	887
				AMOCO 5 (February)			
408.2	275.0	12.41	1800		73.0		
623.6	662.9	13.10	1900		3.49	.10	981
647.4	705.6	↓	↓		2.66	.11	971
673.2	752.0				2.62	.07	946
698.7	797.9				2.38	.06	924
722.7	841.1				2.19	.06	897
				AMOCO 6 (February)			
408.5	275.5	17.24	2500		197		
623.7	662.9	↓	↓		5.26	.42	1032
647.2	705.2				4.93	.40	1021
670.5	747.1				4.46	.32	995
697.4	795.6				3.42	.26	966
723.2	842.0				2.30	.08	938
				AMOCO 8 (April)			
407.2	273.2	17.24	2500		20.8	.60	1071
621.6	659.3	↓	↓		4.20	.15	960
648.2	707.0				3.96	.14	938
672.2	750.2				3.78	.18	917
699.2	798.8				3.67	.15	877
724.2	843.8				2.59	.08	844
698.6	797.9			0	2.32	.02	864
698.2	797.0			50	2.16	.02	855
697.6	796.1			80	2.40	.00	865
698.2	797.0			120	2.33	.00	849

TABLE 1. (Continued)

Temperature K	Temperature °F	Pressure MPa	Pressure psia	Elapsed Time, min	Viscosity η_{pl} mPa·s	Yield Stress, τ_o N/m^2	Density, kg/m^3
				AMOCO 8 (December)			
352.2	174.2	17.24	2500		147		
416.6	290.3	↓	↓		17.1	.53	1092
625.4	666.0				3.30	.25	969
649.2	709.0				3.77	.22	953
672.2	750.2				2.58	.21	923
696.6	794.1				2.41	.15	910
725.0	845.4				2.20	.16	883
				AMOCO 9 (April)			
407.8	274.3	17.24	2500		19.9	.38	1076
624.0	663.4	↓	↓		3.25	.14	956
648.2	707.0				2.60	.14	940
674.4	754.2				2.30	.12	916
699.2	798.8				1.82	.09	881
725.2	845.6				1.81	.04	844
700.2	800.6			0	1.19	.00	850
700.6	801.5			25	1.10	.00	848
701.2	802.4			40	1.15	.00	844
701.4	802.8			55	1.15	-.01	843
701.2	802.4			70	1.09	-.01	841
				AMOCO 9 (December)			
407.4	273.6	17.24	2500		24.0	.48	1120
626.2	667.4	↓	↓		2.71	.25	930
648.8	708.3				2.15	.28	919
650.0	710.4				3.35	.31	912
672.6	750.9				2.33	.34	895
695.6	792.3				2.55	.37	800
695.8	792.7				3.24	.36	881
717.0	830.8				1.80		
				AMOCO 10 (April)			
408.4	275.5	17.24	2500		37.2	1.03	1121
625.6	666.5	↓	↓		3.61	.18	963
648.6	707.9				3.25	.16	937
677.0	758.8				3.01	.13	915
700.6	801.5				1.92	.12	877
724.6	844.7				1.74	.10	838
699.4	799.3			0	1.42	.01	852
699.6	799.7			34	1.31	.01	866
699.2	798.8			63	1.20	.00	864
698.2	797.0			91	1.22	-.01	865
698.8	798.3			137	1.24	.00	865
				AMOCO 10 (January)			
407.0	273.0	17.24	2500		31.0	.53	1122
625.0	665.4	↓	↓		2.08	.18	965
649.2	708.8				1.92	.16	935
673.6	752.7				1.60	.13	917
697.0	794.8				1.64	.12	884
725.4	846.0				1.10	.17	870
				AMOCO 11 (February)			
409.7	277.7	17.24	2500		31.0	.23	1244
620.2	656.6	↓	↓		4.92	.48	1028
649.4	709.2				4.43	.47	1011
672.7	751.1				3.88	.46	990
697.9	796.9				2.95	.41	965
721.4	838.8				2.23	.23	938

TABLE 1. (Continued)

Temperature K	Temperature °F	Pressure MPa	Pressure psia	Elapsed Time, min	Viscosity η_{pl} mPa·s	Yield Stress, τ_o N/m^2	Density, kg/m^3
				AMOCO 12 (February)			
408.2	275.0	17.24	2500		18.4	.49	1067
723.7	662.9	↓	↓		2.81	.08	950
647.7	706.1				2.25	.10	931
672.7	751.1				1.94	—	(906)
698.5	797.5				(2.05)	.11	890
723.5	842.5				1.58	.06	873
				AMOCO 14 (March)			
411.2	280.4	17.24	2500		24.7	1.41	1096
624.0	663.4	↓	↓		1.77	.08	978
647.8	706.3				1.47	.08	949
673.4	752.4				1.18	.05	928
698.0	796.6				.89	.01	897
724.3	844.0				.74	.00	864
				AMOCO 15 (March)			
410.0	278.2	17.24	2500		96.3	.76	1190
626.1	667.2	↓	↓		6.74	.38	1031
650.0	710.2				5.24	.26	1002
674.3	754.0				3.53	.21	975
697.6	795.9				2.88	.18	947
723.3	842.2				2.13	.06	928
				AMOCO 15 (June)			
353.2	176.0	17.24	2500	0			
702.0	805.0	↓	↓	8	4.66	.54	989
694.0	790.0			11	3.74	.51	986
702.6	805.1			18	3.85	.41	978
700.2	800.8			28	3.52	.29	972
702.6	804.9			36	3.24	.24	969
701.2	802.4			60	2.77	.14	955
701.6	803.1			75	2.73	.10	950
702.8	805.3			85	2.73	.08	948
704.0	807.4			100	2.81	.06	941
677.6	760.1			135	2.84	.04	955
649.0	708.6			220	3.12	.04	976
623.4	662.5	↓	↓	257	3.61	.05	988
				AMOCO 16 (March)			
408.7	275.9	17.24	2500		59.9	.88	1220
623.7	662.9	↓	↓		4.92	.11	1028
648.2	707.0				4.14	.11	1012
673.5	752.5				3.49	.11	994
698.5	797.5				2.54	.05	966
724.0	843.4	↓	↓		2.11	.04	956

The plastic viscosity was found to decrease as the temperature increased, as expected. The relationship between yield stress and temperature was not so clear. As will be shown in the next section, the yield stress at any high temperature was found to decrease with time. Therefore a decrease in yield stress with increasing temperature, as was generally observed, may have been due in part to change with time. Nevertheless, there did seem to be some decrease of yield stress with increasing temperature. This effect was relatively small, however. The determination of yield stress at 400 K was not very reliable because of the higher viscosities and the uncertainty in the density.

Changes with Time

The program was devised with the assumption that the samples would not change appreciably with time. It was recognized, however, that changes were possible. Therefore measurements were made as rapidly as possible, starting at lower temperatures and continuing at higher temperatures. In several cases (1, 3, 8, 9, 10) measurements at a lower temperature were repeated after completing the high-temperature work to determine whether any changes had occurred. It was found that both lower plastic viscosities and lower yield stress values were measured after holding at a higher temperature.

On several occasions we held the specimen for a while at constant temperature to determine whether the properties were constant. In general (8, 9, 10) we found a slight decrease in plastic viscosity and a decrease in yield stress. The yield stress at 700 K after previous measurements at 725 K were already low, but they appeared to decrease essentially to zero. AMOCO 1 appeared to be an exception to this behavior. After half an hour at the highest temperature, both plastic viscosity and yield stress were increasing.

At the end of the program, with the opportunity for one more experiment, it was determined to devote this one experiment to a determination of the changes with time at a single temperature. AMOCO 15, previously measured in March, was chosen for this experiment. The sample

was transferred from an autoclave at 353 K to the viscometer at about 700 K. Measurements began immediately but it took about 8 minutes to bring the sample to this temperature. The behavior at 400 K is shown in Figure 3.

The decrease in plastic viscosity seems to be clearly indicated, though the apparent upturn at the end is not so certain. The yield stress changed in a much more pronounced way, decreasing nearly to zero in less than 2 hours. At 425 K the change would, no doubt, be more rapid. The change in density was unexpected. The change was about 5 percent, which is a substantial change. The data seem to indicate this change clearly. We are not sure what to make of it.

The data obtained during sample heatup, while not sufficient for treatment in the usual way, indicate a thickening of the sample, whether caused by an increase in plastic viscosity or an increase in yield stress is not clear. This time period was difficult to interpret because rising temperatures were changing density and therefore buoyancy of the bob. Therefore we cannot be sure about this apparent transitory phenomenon.

One more peculiarity in the data should be pointed out. For AMOCO Samples 1 and 2 the trend with time and for yield stress even with temperature seems to be the reverse of that generally observed. Each sample was run twice, and in each of the four runs there appears to be an upward trend in yield stress.

Effect of Pressure

For several samples measurements were made at pressures of 13.8, 17.2 and 20.7 MPa of hydrogen. No discernible trend was detected. Previous experience with similar but much more viscous materials indicates that the pressure effect might have been expected to be about 5 percent for a 1000 psi change -- higher viscosity for the higher pressure. The scatter in our data was often greater than that.

Replication

In all, six of the determinations were repeated. The scatter was great, even after the January corrections. Furthermore, in most cases the earlier results in plastic viscosity were consistently lower than the later. The average difference between the earlier and later determinations ranged from 11 percent for AMOCO 1 to 36 percent for AMOCO 10. Sample 1 is said to be the same as Sample 2; similarly Samples 8 and 9 were duplicates. Each of these four was run twice. The deviations between the pairs in each case were of the same order of magnitude as deviations between repeat runs.

A similar comparison between repeat determinations of yield stress shows a similar level of agreement. At higher temperatures the agreement is worse, presumably as the yield stress decreased with time for each measurement.

In general we would have to say that the agreement between repeat determinations was less good than we had hoped. This is only party due to uncertainties regarding the condition of the sample, such as the possible separation of solids before transferring the sample to the viscometer, uncertainties in the extent of change brought about by standing at high temperature and the like. A large part of the uncertainty seems to be due to instrumental problems such as the lack of alignment.

Comparison with ORNL Results

It is our understanding that the correspondence of samples used by ourselves and ORNL is as shown in Table 2. Because of the changes with time we have shown also our yield stress results at 700 K, which we judge to be closer to the value at zero time than the value determined at 725 K.

Although the order of magnitude of the results was the same as determined by the two methods, the agreement is not very close. Especially in the case of AMOCO 11 and Sample 43A the results are in serious disagreement, even in density. Because of the rapidity of changes with time, which is no doubt greater at 725 K than shown in Figure 3 at 700 K, and because of the differences in residence time for the two methods, the differences

TABLE 2. COMPARISON OF RESULTS AT 725 K

ORNL Results				
Sample Number	27B	34A	42A	43A
η_{pl}, mPa·s	1.68	3.03	1.73	1.07
τ_o, N/m^2	.126	.307	.232	.192
ρ, kg/m^3	908	985	882	851
This Research				
Sample Number	5	6	9	11
η_{pl}, mPa·s	2.19	2.30	1.81	2.23
τ_o at 725, N/m^2	.06	.08	.04	.23
τ_o at 700, N/m^2	.06	.26	.09	.41
ρ, kg/m^3	897	938	844	938

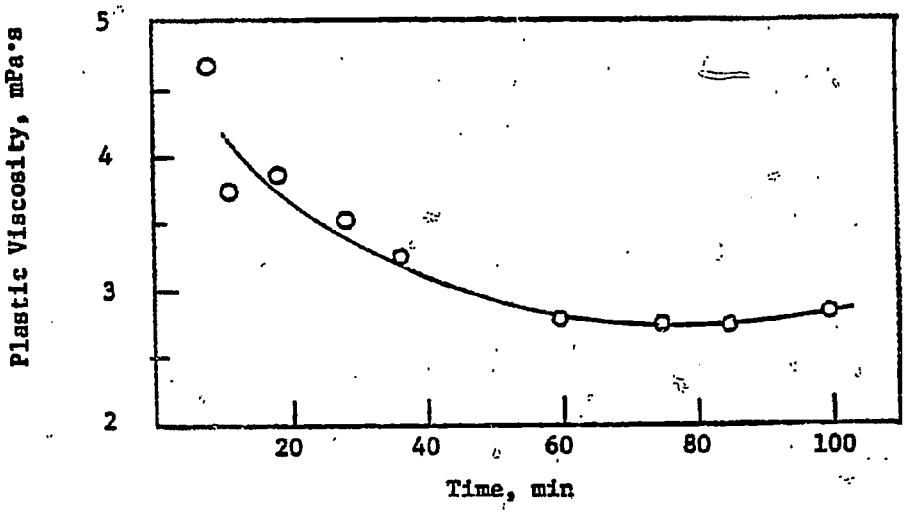

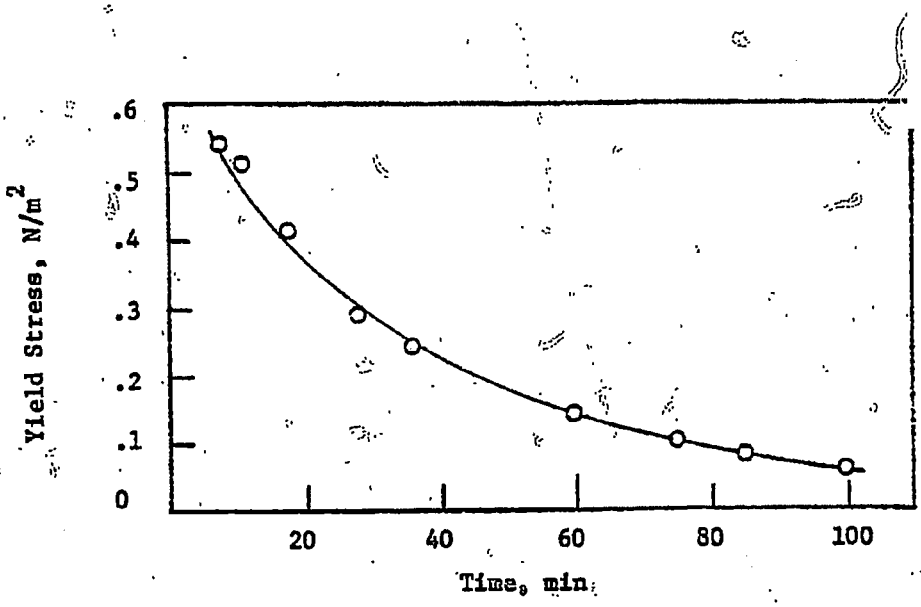

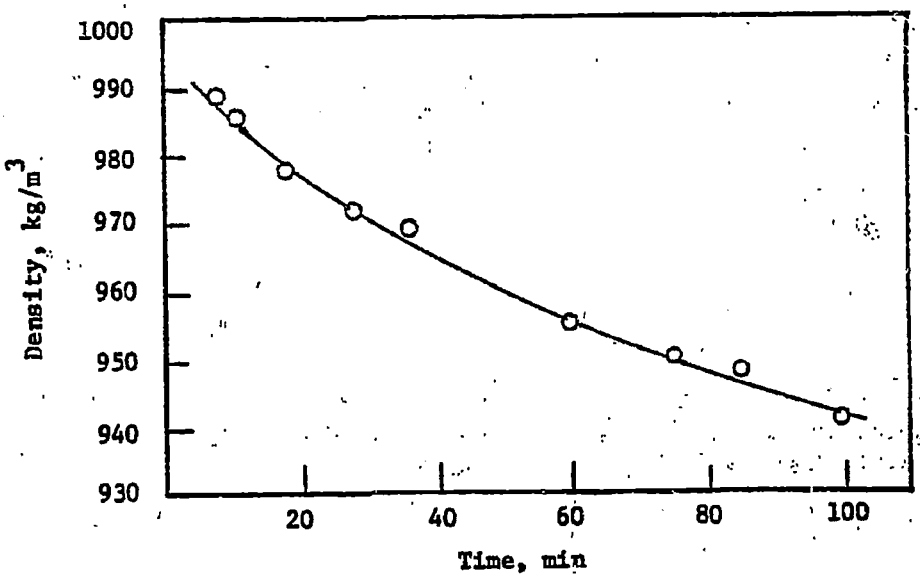

FIGURE 3. VISCOUS PROPERTIES OF AMOCO 15 AT 700 K

in results were perhaps no greater than should be expected. Even so, the differences between 11 and 43A seem to be excessive.

FUTURE WORK

Further determinations of rheological properties of samples such as those examined in this program would have to be based on an experimental design that deals with the changes in properties with time. Experiments similar to the one illustrated in Figure 3 could be used to extrapolate results back to zero time. With a little practice we believe that usable results could be obtained within 2 or 3 minutes of the transfer. Similar measurements at other temperatures would aid in interpretation of the results.

Further development of the instrument, together with some stable samples with which to make comparisons, should lead to greater confidence in the results.

REFERENCES

(1) Castillo, C. and Williams, M. C., "Rheology of Very Concentrated Coal Suspensions", Chem. Eng. Commun., (3), 529-547 (1979).

(2) Bhattacharya, S. N. and Barro, L., "Rheology of Aging of Coal-Oil Suspensions", Rheology (Proceedings of 8th International Congress), 1980, 2, 615-621.

(3) Krzyzanowska, T. and Marzec, A., "Coal-Derived Group Component Effects on Viscosity", Fuel, 57, 804-805 (1978).

(4) Bockrath, B. C., Lacount, R. B., and Noceti, R. P., "Coal-Derived Asphaltenes: Effect of Phenol Content and Molecular Weight on Viscosity of Solutions", Fuel, 59, 621-626 (1980).

(5) Brown, F. R. and Karn, F. S., "Stability Studies of Coal Liquids", PETC/TR-79/5.

(6) Oswald, G. E., Youngblood, E. L., and Hightower, J. R., Jr., "Rheological Characterization of Coal-Solvent Slurry at High Temperature and Pressure", AIChE Meeting, Philadelphia, Pennsylvania, June 8-12, 1980.

REFERENCES
(Continued)

(7) Droege, J. W., Hassell, J. A., and Chauhan, S. P., "Viscosity at Elevated Temperature and Pressure of Coal-Derived Liquids", Proc. 7th Symp. Thermophysical Prop., Gaithersburg, Maryland, May 10-12, 1977, ASME.

(8) Smith, T. L., Ferry, J. D., and Schremp, F. W., J. Appl. Phys., 20, 144-153 (1949).

Battelle
Columbus Laboratories
505 King Avenue
Columbus, Ohio 43201
Telephone (614) 424-6424

APPENDIX B

NORTHWESTERN UNIVERSITY PROGRESS REPORTS

MONTHLY (APRIL 1981) PROGRESS REPORT ON AMOCO DOE CONTRACT "ON H-COAL FLUID DYNAMICS"

AMOCO Project Status

Work for the past month on the light beam bubble probe has focused primarily on making the probe operational in the column. Initial difficulties were encountered in obtaining propagation of the beam through the probe tips with a surrounding fluid environment. A redesign of the tip (see attached figure) to include an optical fiber window and screw together assembly has eliminated the problem of bubbles within the tip blocking the optical path. Fluid is used on both sides of the optical fiber window to reduce the effects of not having optically flat and parallel ends on the fibers.

Another problem which has been overcome is excessive noise level (equal to that of the signal) when the bed is fluidized above the probe level. This has been solved by making the receiving optics insensitive to small deflections of the light beam caused by propagation through the glass particles. The cure was to use a lens to focus the light to point on the end of a 1. mm diameter optical fiber.

With the bed fluidized and the fluid temperature within approximately 1^{o} F of the optimum value, we now have signal to noise ratios of about 3 or 4 to 1. This noise seems primarily due to scattering of light at the fluid-particle interfaces and the resulting loss in beam intensity.

Visual observation of the signal on an oscilloscope is encouraging and we are now directing our attention to developing the necessary data collection and analysis programs.

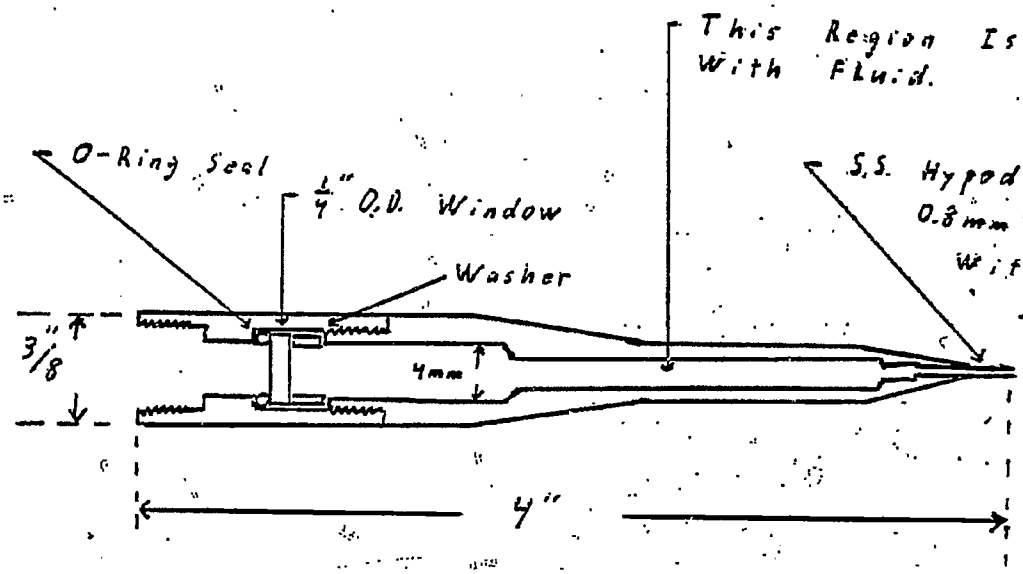
This Region Is Filled With Fluid.
O-Ring Seal
¼" O.D. Window
Washer
S.S. Hypodermic Tubing, 0.8mm O.D., 10mm Long, with Glass Fiber Inside
3/8"
4mm
4"

MONTHLY (MAY 1981) PROGRESS REPORT ON AMOCO DOE CONTRACT "ON H-COAL FLUID DYNAMICS"

(I) Impendance Probe

For the past two months, most work done is attributed to modifying the probe circuit and to finding a way to record digital data on floppy disk.

The magnitude of the output signal from the probe depends mostly on the surface area of the tip of the probe. Since the tip diameter of the new probe (0.01") is only half of that of the old probe, the gain from the circuit has to be increased in order to get a satisfactory signal output.

Two independent circuits are also constructed. Circuit A can be used to set single threshold, while circuit B is used to set double threshold. The voltage levels of the two thresholds are 0.6 V and 3.0 V respectively. Hence, the magnitude of the output signal must be greater than 2.4 V whenever circuit B is used.

(II) Light Probe

Work during May on the light beam probe for bubble size and void fraction determination focused on writing the computer programs for collecting and analysing the data. Improvements will continue to be put into the programs, but they are now operational and running smoothly. A small amount of preliminary data has been collected and the method seems promising. Included in this report is a description of the basic concepts of the light beam probe, as shown in Appendix A.

Appendix A

BASIC CONCEPTS OF THE LIGHT BEAM PROBE FOR DETERMINING VOID FRACTION AND BUBBLE SIZE DISTRIBUTIONS

Paul R. Geernik

Northwestern University

June 8, 1981

INTRODUCTION

The basic thought behind the ideas presented below is that the distance one can see through a two-phase mixture depends upon both the void fraction and the size distribution of the bubbles involved. The presentation is broken up into two main parts:

1. Determination of the void fraction assuming the size distribution is known
2. Determination of the size distribution and average velocities.

A glossary of symbols follows the presentation.

VOID FRACTION DETERMINATION

To begin with, consider a hypothetical two-phase flow in which the gas volume fraction, α, consists entirely of bubbles with a known radius, r_b. For this case it is a very simple task to calculate the void fraction. It is only necessary to determine the average number of bubbles which would intersect an infinitesimally thin line of a known length passing through the fluid. To see how this can be done replace each bubble by a point and expand the radius of the line to r_b. The number of points lying within the volume of this "thick" line will then be equal to the number of bubbles which would have intersected the narrow line.

Let n = the number of bubbles per unit volume

$N(r_b)$ = average number of bubbles of radius r_b intersecting a line of unit length

Then, $$n = \alpha/(4\pi r_b^3/3) \qquad (1)$$

and $$N(r_b) = \pi r^2 n = 3\alpha/4r \qquad (2)$$

Thus, for this simple case, if the radius of the bubbles were known along with the average number of bubbles which intersected a line of unit length, the void fraction could be determined.

To measure the quantity $N(r_b)$, a narrow light beam (radius less than the bubble radius) could be passed through a length ℓ of the fluid and its transmitted intensity monitored. By using a small receiving aperture, any portion of the beam intersecting a bubble will be deflected outside of this aperture. Therefore, when a bubble has cut more than halfway through the beam the received intensity will fall below half of full scale and the beam axis (which is an infinitesimally thin line) can be considered "broken".

Whenever the transmitted intensity is sampled and found to be greater than half of full scale, what has actually been done is to have taken a sample of a given path length, ℓ, of fluid and found it to intersect no bubbles. If this sampling is done multiple

times a determination is made of the fraction of paths which have clear path lengths greater than ℓ. The mean clear path length is

$$\lambda = 1/N(r_0) \qquad (3)$$

and from elementary statistical theory, the fraction of paths with a clear path length greater than a given distance ℓ, will be

$$f = \exp(-\ell/\lambda) = \exp(-\ell N(r_0)) \qquad (4)$$

Thus, if the fraction of time the beam is not broken is known, we have

$$N(r_0) = -\ln(f)/\ell \qquad (5)$$

and the void fraction is given by

$$\alpha = -4r_0 \cdot \ln(f)/3\ell \qquad (6)$$

The above result is not of much practical use however, so the next step is to generalize the above ideas. Define

$\alpha(r)dr$ = volume fraction of those bubbles which have radii between r and r+dr

$N(r)dr$ = average number of bubbles with radii between r and r+dr that intersect a line of unit length

Then, from equation (2),

$$N(r)dr = (3\,\alpha(r)/4r)dr \qquad (7)$$

Integrating this over all possible r values,

$$N_T = \int_0^\infty N(r)dr = \int_0^\infty (3\,\alpha(r)/4r)dr \qquad (8)$$

which is the generalization of equation (2).

For this more general case, N_T can be determined the same way $N(r_0)$ was before, but now it is also necessary to know the shape of the void fraction distribution curve. The proceedure for calculating this is covered in the next section.

CALCULATING THE VOID FRACTION DISTRIBUTION

To determine the void fraction distribution it is necessary to obtain more information from the transmitted light intensity than just the fraction of time that the beam is broken. The other information available consists of the duration of the beam breaks and the rate at which the beam is cut off. These two quantities depend upon the following three variables:

1. r = the bubble radius

2. s = the distance of closest approach measured from the bubble center to the beam axis

3. v = the speed of the bubble in the plane perpendicular to the light beam

For the following analysis, two assumptions will be made:

1. The bubbles are spherical

2. During the time that a given bubble breaks the light beam, it travels in a straight line at a constant speed.

And define:

$g(r,v)$ = fraction of time per unit speed that a bubble of radius r would have a speed v in the plane perpendicular to the light beam.

r_0 = radius of the light beam

$R(r,v,s)drdvds$ = the relative frequency at which bubbles with
a) radii between r and r+dr
b) speeds between v and v+dv
c) and closest approach distances between s and s+ds
break the beam

Now make the stipulation that data obtained from the passage of a given bubble through the beam will only be counted if the transmitted light intensity falls all the way to zero. With this restriction, all values of s between 0 and $(r-r_0)$ should be equally likely and the probability of accepting data for which $s > (r-r_0)$ will be zero. In other words,

$$R(r,v,s)drdvds \sim ds \quad \text{for } 0 \leq s \leq (r-r_0)$$

$$= 0 \quad \text{for } s > (r-r_0) \qquad (9)$$

It should also be clear that the relative frequency function will be proportional to

1) the number density of bubbles with radii between r and r+dr, which is given by

$$\propto (r)dr/(4\pi r^3/3)$$

2) the fraction of those bubbles of size r which have speeds between v and v+dv, which is given by

$$g(r,v)dv$$

3) and finally the speed of the bubbles, which is given (of course) by

$$v$$

Therefore,

$$R(r,v,s)drdvds \sim (3\alpha(r)dr/4\pi r^3)(g(r,v)dv)(v)(ds) \quad (9)$$

Since we are concerned only with the relative frequency, the constant factors can be dropped and the following equality made

$$R(r,v,s)drdvds = (\alpha(r)/r^3)g(r,v)vdrdvds \qquad 0 \leq s \leq (r-r_0)$$
$$= 0 \qquad s > (r-r_0) \quad (10)$$

Now that an expression for the relative frequency function has been determined, the next step is to determine exactly what information can be extracted from the light beam signal as a bubble with particular r, v, and s values passes through the beam. In the following figure, the light beam is perpendicular to the plane of the paper and the asterisks represent the position of the beam relative to the bubble at various points in time.

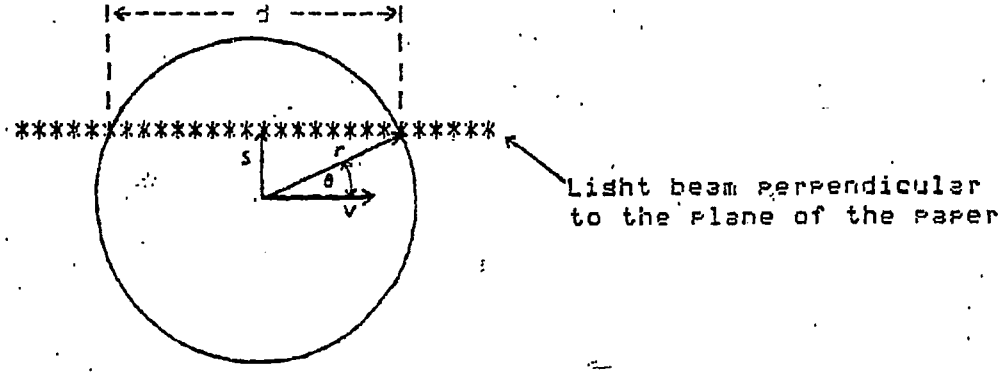

$$d = 2\sqrt{r^2 - s^2} \quad (11)$$

The quantity d is the distance that the bubble travels while the beam is broken, so the time duration of this break will be

$$\tau = d/v = 2(r^2 - s^2)^{1/2}/v \quad (12)$$

In addition to the duration of the break, the rate at which the light intensity is cut off is also available. If the intensity profile of the light beam is known (for the helium-neon laser it will be a gaussian profile), this transmitted intensity vs. time data can be converted to yield the bubble interface position vs. time. Thus the speed u at which the bubble cuts off the light beam can be determined.

This calculated speed, u, will in general not be the same as v, but rather

$$u = v\cdot\cos\theta \qquad (13)$$

where $\theta = \cos(d/2r) \Rightarrow u = v(r^2-s^2)^{1/2}/r \qquad (14)$

To see this relationship more clearly, consider

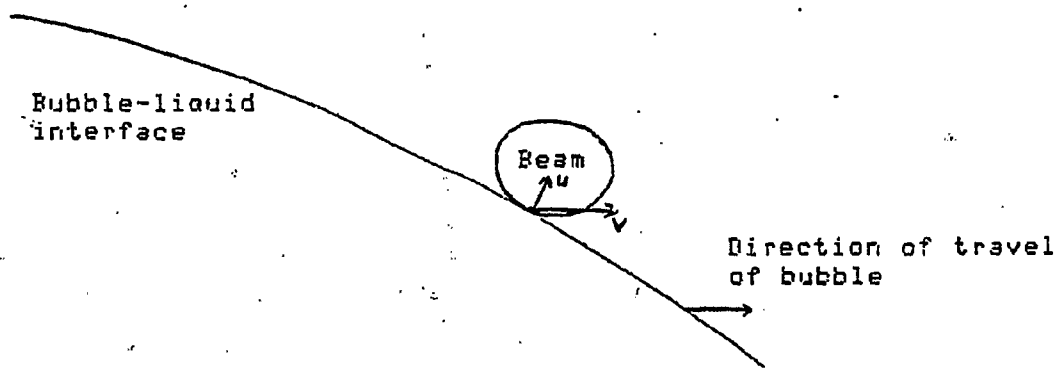

There is a component of bubble velocity which merely moves the bubble surface parallel to the beam 'surface', and thus plays no part in cutting off the beam. Only the component of the bubble velocity perpendicular to the bubble surface at the point of intersection with the beam plays an effective role.

To summarize, the information which can be obtained from each passage of a bubble through the beam is

$$\tau = 2(r^2-s^2)^{1/2}/v \qquad (12)$$

$$u = v(r^2-s^2)^{1/2}/r \qquad (14)$$

The next step towards determining the void fraction distribution is to organize this available data in some logical manner. To do this, define and consider the quantity

$$p = \tau u/2 = r(1-s^2/r^2) \qquad (15)$$

For the case of $s=0$, p would equal the radius of the bubble passing through the beam. For $0 \leq s \leq (r-r_b)$,

$$r_b(2-r_b/r) \leq p < r \qquad \text{where } r \geq r_b \qquad (16)$$

With this information in mind, define a function

$Q(a)$ = frequency at which bubbles break the beam such that $p \leq a$

Analytically, $Q(a)$ will be proportional to the integral of $R(r,v,s)$ over all possible values of r, v, and s, subject to the constraint

$$p \leq a$$

$$\text{or} \qquad r(1-s^2/r^2) \le a \;\Rightarrow\; s \ge \sqrt{r^2-ra} \quad \text{for } r \ge a \qquad (17)$$
$$s \ge 0 \quad \text{for } r < a$$

To simplify the notation, define

$$z = \sqrt{r^2-ra} \quad \text{for } r \ge a \qquad (18)$$
$$= 0 \quad \text{for } r < a$$

Thus, using equation (10)

$$Q(a) = A\int_{r_b}^{\infty} dr \int_{z}^{r-r_b} ds \int_{0}^{\infty} dv\, \alpha(r) g(r,v) v/r^3 \qquad (19)$$

where A is a normalization constant. Since we are actually only interested in the shape of the Q function, redefine Q by equation (19) with A=1. The value r_b is the lower limit for the integration over r since bubbles with radii less than the beam radius are not capable of totally blocking off the light beam.

Now if we define average speed as

$$\bar{v}(r) = \int_{0}^{\infty} g(r,v) v dv \qquad (20)$$

equation (19) becomes

$$Q(a) = \int_{r_b}^{\infty} dr \int_{z}^{r-r_b} ds\, \alpha(r)\bar{v}(r)/r^3 \qquad (21)$$

This can be rearranged to

$$Q(a) = \int_{r_b}^{\ell} dr \int_{0}^{r-r_b} ds\, \alpha(r)\bar{v}(r)/r^3 + \int_{\ell}^{\infty} dr \int_{\sqrt{r^2-r\ell}}^{r-r_b} ds\, \alpha(r)\bar{v}(r)/r^3$$

$$= \int_{r_b}^{\ell} dr(r-r_b)\,\alpha(r)\bar{v}(r)/r^3 + \int_{\ell}^{\infty} dr\left[(r-r_b)-\sqrt{r^2-ra}\right]\alpha(r)\bar{v}(r)/r^3$$

$$= \int_{r_b}^{\infty} \left[(r-r_b)\,\alpha(r)\bar{v}(r)/r^3\right]dr - \int_{\ell}^{\infty} \left(\sqrt{r^2-ra}\,\alpha(r)\bar{v}(r)/r^3\right)dr \qquad (22)$$

Equation (22) is the integral spectrum of frequency vs. a. Taking the derivative with respect to a yields the differential spectrum.

$$dQ/da = \int_{\ell}^{\infty} \left[r\,\alpha(r)\bar{v}(r)/2\sqrt{r^2-ra}\cdot r^3\right]dr \qquad (23)$$

Now, since once again only the shape of the curve is important, eliminate the constant factor. Also convert from the variable a back to ρ and define

$$M(\rho) = \int_{\rho}^{\infty} [\alpha(r)\bar{v}(r)/r^2\sqrt{r^2-r\rho}]\,dr \qquad (24)$$

The important characteristic of the above equation is that $M(\rho)$ involves only the integral over values of $r \geq \rho$. If the ρ axis is broken up into discrete intervals, it is then possible, starting at the highest interval, to calculate the void fraction corresponding to the different ranges of bubble sizes.

For an example, consider again the simplest case where all the bubbles are of the same radius. This implies that

$$\alpha(r) = \alpha_0(r-r_b)$$

Then
$$\begin{aligned} M(\rho) &= 0 && \text{for } 0 \leq \rho \leq r_b(2-r_b/r_0) \\ &= \alpha_0\bar{v}(r_0)/r_0^2\sqrt{r^2-r\rho} && \text{for } r_b(2-r_b/r_0) < \rho < r_0 \\ &= 0 && \text{for } \rho > r_0 \end{aligned} \qquad (25)$$

The reason $M(\rho)=0$ for $0 \leq \rho \leq r_b(2-r_b/r_0)$ is due to the stipulation that $s \leq (r-r_b)$, as was stated in arriving at equation (16).

Graphically, $M(\rho)$ for this simple case, with the further specification that $r_0 = 7r_b$, appears on the following page.

To make use of equation (24) to calculate $\alpha(r)$, it is necessary to know $\bar{v}(r)$. To see how $\bar{v}(r)$ can be determined, divide equation (13) by equation (11), and obtain

$$u/\tau = v/2r \;\Rightarrow\; v = (2ru/\tau)^{1/2} = \sqrt{2r}\,(u/\tau)^{1/2} \qquad (26)$$

The quantity u/τ is independent of s, and therefore it is possible to calculate the average value of $(u/\tau)^{1/2}$ for bubbles of a given size from the available data (the method of doing this is given below). The one additional step of multiplying by $\sqrt{2r}$ will then give $\bar{v}(r)$.

The final major step in determining the void fraction distribution is to consider the practical algorithm required. First, it is necessary to discritize the ρ axis and define a linear array $\underline{M}$ whose dimension equals the number of intervals into which the ρ axis is divided. Every time a bubble passes through the beam the values of u and τ will be determined, and the value of $\rho = \tau u/2$ calculated. Then the element of array $\underline{M}$ which corresponds to the interval into which this ρ falls will be incremented.

It is also necessary to store the velocity information, namely $\sqrt{u/\tau}$, obtained from each bubble. For this purpose, another array, $\underline{U}$, with the same dimension as $\underline{M}$, needs to be defined.

(12)

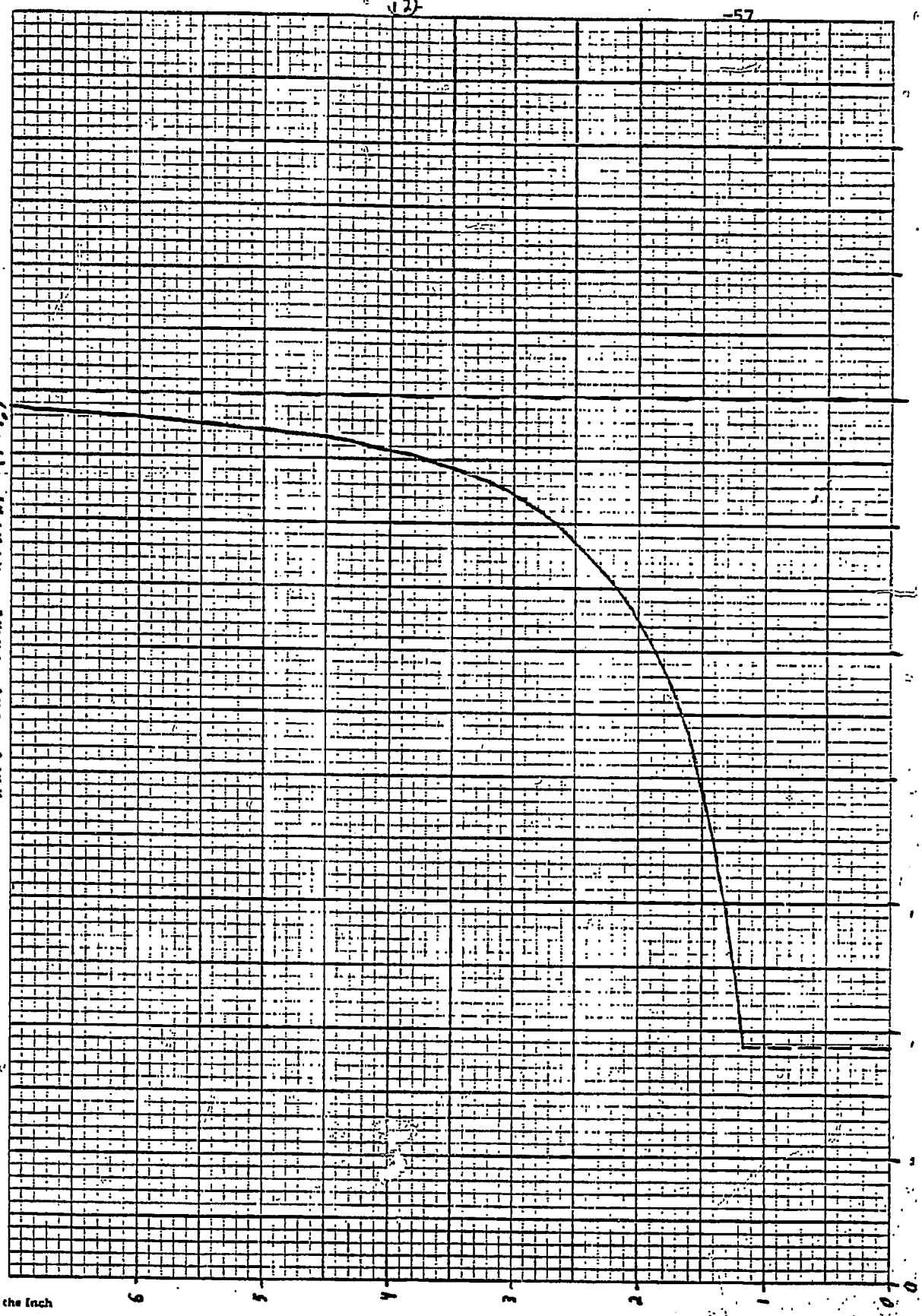

squares to the inch

$M(p)$ = units are $\sigma\sqrt{(p)}/r_0^3$

Into the element of this array corresponding to the calculated ρ value would be added the quantity $\sqrt{u/\tau}$, from each bubble.

After a sufficient ammount of data has been accumulated, it must be analyzed it to obtain the quantities $\alpha(r)$ and $\bar{v}(r)$. In the highest ρ interval which has a non-zero entry in the M array, all the data points can be considered to have been generated by bubbles passing centrally through the light beam with radii equal to the ρ value of the interval. Consequently, the value of $\bar{v}(r)$ can be determined by dividing the proper element of the $\underline{U}$ array by the corresponding element of the $\underline{M}$ array, and multiplying by $\sqrt{2r}$. Now, if $\alpha(r)$ is assumed to be constant over this ρ interval, $\rho_{L-1} \leq \rho \leq \rho_L$, then

$$\underline{M}(\rho_L) = \int_{\rho_{L-1}}^{\rho_L} M(\rho)d\rho = \int_{\rho_{L-1}}^{\rho_L} d\rho \int_{\rho}^{\rho_L} [\alpha(r)\bar{v}(r)/r^2\sqrt{r^2-\rho^2}\,]dr$$

$$= \alpha(r_L)\bar{v}(r_L)\int_{\rho_{L-1}}^{\rho_L} d\rho \int_{\rho_{L-1}}^{r} [1/(r^2\sqrt{r^2-\rho^2}\,)]d\rho$$

$$= \alpha(r_L)\bar{v}(r_L)\int_{\rho_{L-1}}^{\rho_L} d\rho[-2\sqrt{r^2-\rho^2}\,/r^3\,]$$

$$= \alpha(r_L)\bar{v}(r_L)\int_{\rho_{L-1}}^{\rho_L} [\sqrt{r^2-\rho^2}\,/r^3\,]dr$$

Let $$I_L = \int_{\rho_{L-1}}^{\rho_L} [\sqrt{r^2-\rho^2}\,/r^3\,]dr \qquad (26)$$

Then $$\alpha(r_L) = \underline{M}(\rho_L)/(\bar{v}(r_L)I_L) \qquad (27)$$

Now, bubbles of size r_L passing through the beam off center will have resulted in data being accumulated in the lower elements of the $\underline{M}$ and $\underline{U}$ arrays. The statistically expected amount of 'pollution' in the lower elements must be subtracted out before proceeding with the calculation of $\bar{v}(r_{L-1})$ and $\alpha(r_{L-1})$. The expected number of counts in the Kth interval due to bubbles whose radii fall in the Lth interval will be

$$X_{K,L} = \int_{\rho_{K-1}}^{\rho_K} d\rho \int_{\rho_{L-1}}^{\rho_L} [\alpha(r)\bar{v}(r)/r^2\sqrt{r^2-\rho^2}]dr$$

$$= \int_{\rho_{L-1}}^{\rho_L} d\rho \int_{\rho_{K-1}}^{\rho_K} [\alpha(r)\bar{v}(r)/r^2\sqrt{r^2-\rho^2}]d\rho$$

$$= \alpha(r_L)\bar{v}(r_L)\int_{\rho_{L-1}}^{\rho_L} d\rho[-2\sqrt{r^2-\rho^2}\,/r^3]\Big|_{\rho_{K-1}}^{\rho_K}$$

$$= 2\alpha(r_L)\bar{v}(r_L)\int_{\rho_{L-1}}^{\rho_L}\left[\sqrt{r^2-r\rho_{K-1}}-\sqrt{r^2-r\rho_K}\right]/r^3\,dr$$

Let $$I_{K,L} = 2\int_{\rho_{L-1}}^{\rho_L}\left[\sqrt{r^2-r\rho_{K-1}}-\sqrt{r^2-r\rho_K}\right]/r^3\,dr$$

then, $$X_{K,L} = \alpha(r_L)\bar{v}(r_L)I_{K,L}$$

This value of $X_{K,L}$ must be subtracted from the Kth element of the $\underline{M}$ array, and the quantity

$$X_{K,L}\left[\sum_{bubbles} u/\tau\right]/\underline{M}(\rho_L)$$

must be subtracted from the Kth element of the $\underline{U}$ array. Once the data in the lower elements of the $\underline{M}$ and $\underline{U}$ arrays has been corrected, the above analysis process can be repeated to determine the $\alpha(r_{L-1})$ and $\bar{v}(r_{L-1})$ values, and so on down to the smallest interval.

SUMMARY

The procedure described here for determining $\alpha(r)$ would yield exact results if an infinite amount of data were collected on bubbles which satisfied the two assumptions made in the analysis.

1. The bubbles are spherical
2. They move in a straight line at a constant speed while they break the beam.

The limitations on accuracy due to a finite amount of data will depend upon the distribution of bubble sizes, especially in the lower size ranges. Obviously, if 99% of the data accumulated in a given ρ int-interval (ρ_L) were due to bubbles whose radii fell in higher intervals, the relative accuracy of $\alpha(\rho_L)$ would be very poor.

The limitations imposed by the two assumption about the bubbles will need to be determined by comparing the values of u calculated from entrance and exit data. If the assumptions are satisfied, the values in each pair of velocity data should match closely.

GLOSSARY OF SYMBOLS

d = distance a bubble travels while the light beam is broken

$f(\ell)$ = fraction of clear path lengths greater than

$g(r,v)$ = bubble speed distribution function

ℓ = path length of light beam

$M(p)$ = frequency per unit p about p, at which bubbles break the light beam

n = number density of bubbles

$N(r)$ = average number of bubbles intersecting a line of unit length

p = $\tau u/2$ = apparent bubble radius

Q = frequency at which bubbles break the beam such that p Q

r = bubble radius

r_b = light beam radius

$R(r,v,s)$ = relative frequency function

s = distance of closest approach of the bubble center to the beam axis

u = apparent bubble speed

v = bubble speed

α = void fraction

λ = mean clear path length in the fluid

τ = time duration of the bubble in the light beam

L,K = subscripts

ARRAYS

M = array in which bubble frequency data as a function of p is accumulated

U = array in which bubble speed data as a function of p is accumulated

$X_{k,L}$ = number of counts accumulated in M for the p interval $p_{k-1} \leq p \leq p_k$ due to bubbles of size $r_{L-1} \leq r \leq r_L$

MONTHLY (JUNE 1981) PROGRESS REPORT ON AMOCO DOE CONTRACT "ON H-COAL FLUID DYNAMICS"

Work on the light beam probe has concentrated on optimizing the optics of the probe and improving the data analysis procedure. We want to insure that a radially symmetric light beam is passed through the fluid so that our measurements are as accurate as possible. One improvement which would help to give us a consistently good beam would be to use a single-mode optical fiber to carry the beam into the input probe. This would also greatly simplify alignment problems. We are hoping to obtain some single-mode fiber through International Telephone and Telegraph Corporation.

Work is also being done on a revised data analysis procedure which would yield the size and velocity of each bubble as it passed through the beam. The idea is to take advantage of the change in the apparent speed of bubbles which pass through the beam off center. The speed which is measured by the probe is the component of the bubble speed along the line between the beam axis and the bubble center. Since the angle between this line and the bubble velocity vector changes as the beam is cut off, the apparent speed will also change. As may be guessed, the primary difficulty with this method is measuring the changes in apparent speed accurately enough. At this point it does not appear to be unreasonable to spend some time on this method, especially since questions on the accuracy of the measurements must be answered.

The holographic system was checked to determine its alignment and depth of field by taking a hologram of bubbles rising in the test section. The liquid was at rest. Because of the low gas flow rate, the bubble concentration was also low. It was possible in these tests to observe the bubbles on the hologram and measure their size over the entire 6" of the test section. The image

formed by the hologram is magnified two-fold by the lens system. To enhance the viewing of the reconstructed image, the holographic plate was moved closer to the planes where the images are formed. We will take holograms of flows having high concentration of small bubbles in order to determine the limits of application.

Finally, since it is clear that fluid properties play a major role in determining bubble sizes, we have ordered the necessary parts to set up a 3" I.D. column in which it will be much easier to change fluids.